Coverage Analysis of Single-swarm mmWave UAV Networks under Multiple Types of Blockages

Cunyan Ma, Xiaoya Li, Chen He, Jinye Peng, Kun Yang, and Z. Jane Wang, *Fellow, IEEE*

***Abstract*—Millimeter wave (mmWave)-based unmanned aerial vehicle (UAV) communication is susceptible to blockages, even from humans. Previous studies that primarily focused only on static blockage may not accurately characterize the system performance. This paper investigates the coverage performance of mmWave UAV networks by jointly considering multiple types of blockages under finite homogeneous Poisson point process and Binomial point process, which are commonly employed in finite area scenarios with random and fixed number of UAVs, respectively. Particularly, we derive the average line-of-sight probability and coverage probability under static, dynamic, and self blockages. Simulations verify our theoretical results, demonstrating that: the above system performance predominantly depends on self-blockage if UAVs are at high altitudes. Conversely, at relatively low altitudes, all three types of blockages impact them, with static blockage being the dominant factor. To avoid self-blockage, UAV height should satisfy $h > h_R + \frac{r_i}{\tan \varphi_b}$, where h_R is the height of the user equipment (UE), r_i is the two-dimensional distance of the UAV-UE link, φ_b is the elevation angle between UE and UAV. The required height is proportional to r_i and increases as distance d between the user and UE decreases, as φ_b is proportional to d. The findings help on designing the network parameters. To our best knowledge, this is the first work to analyze the coverage of mmWave UAV networks under multiple types of blockages.**

***Index Terms*—Millimeter wave, unmanned aerial vehicle communications, human blockages, coverage probability.**

I. Introduction

A. Motivation

Unmanned aerial vehicles (UAVs) are increasingly recognized as crucial components of wireless communications, particularly as aerial base stations (BSs) [1]. Compared to traditional BSs, UAVs have high mobility and low costs [2], [3]. These facilitate dynamic deployment based on real-time demands and lightweight deployment with lower geographical requirements [4], [5]. Therefore, UAVs are promising candidates to deal with wireless coverage issues, especially for hot spots or disasters [6]. Since UAVs are often used for emergency and temporary communications, most UAVs need fast responses and high transmission rates [7], [8]. Therefore, millimeter wave (mmWave) with large bandwidth is a suitable carrier frequency for UAV communications [8], [9].

This work was supported in part by the National Natural Science Foundation of China under Grant 62271392 and 61901375, the China Postdoctoral Science Foundation under Grant 2019M663950XB. Cunyan Ma and Xiaoya Li contributed equally to this work. (Corresponding author: Chen He).

Cunyan Ma, Xiaoya Li, Chen He, and Jinye Peng are with the School of Information Science and Technology, Northwest University, Xi'an 710127, China (e-mail: chenhe@nwu.edu.cn).

Kun Yang is with the School of Computer Science and Electronic Engineering, University of Essex, Colchester CO4 3SQ, U.K.

Z. Jane Wang is with the Department of Electrical and Computer Engineering, The University of British Columbia, Vancouver, BC V6T1Z4, Canada.

Nevertheless, mmWave UAV communications encounter serious blockages since mmWave are sensitive to obstacles and typically encounter three types of blockages: static blockage due to buildings, dynamic blockage due to moving blockers, and self-blockage due to the user's body [10]–[15]. These blockages pose challenges to the reliability of mmWave UAV communications [5]. Existing research in this field has taken part of these blockage effects into account [7], [10], [16]–[18]. Particularly, the work in [16] focused on enhancing air-to-ground transmission by utilizing intelligent reflecting surface. However, existing works on the coverage performance of mmWave UAV networks primarily considered static blockage, the dynamic and self blockages have not been jointly considered yet. This is unreasonable and will result in considerable deviations from actual performance. Particularly, mmWave are not only sensitive to blockages of buildings, but also sensitive to those of humans, which can lead a signal strength reduction as large as 20 dB [11], [12], [14], [19]. Moreover, since UAVs are typically deployed in hot spots that contain a large number of humans [12], [20], the possibility of blockage caused by humans is further increased. Therefore, it is crucial to jointly considering all three types of blockages. This will provide a better understanding of the coverage performance and ensure more accurate assessment of the network deployment.

Stochastic geometry is widely used to evaluate the system performance and the impact of key parameters on the system performance [21]–[23]. Most existing works in this field models the positions of UAVs using the homogeneous Poisson point process (HPPP). However, when a fixed number of UAVs is deployed, the HPPP model is unsuitable, and the Binomial point process (BPP) is considered as a reasonable model [24]. The system performance varies in different modes since various point processes comprise different numbers of UAVs. Thus, it is necessary to explore the system performance under these two models for different numbers of UAVs, which leads to a variety of challenging mathematical analysis. Consequently, one of our objective is to investigate the coverage performance of air-to-ground mmWave UAV networks under these two different UAV distribution modes to determine UAV distribution models suitable for different scenarios.

B. Related Works

The evaluation of UAV networks performances using random point processes has garnered increasing attention. Most of these studies focus on analyzing the signal-to-interference-plus-noise ratio (SINR) coverage performance and revealing the impact of key parameters on the performance. For instance,

based on HPPP, the work in [25] investigated the impact of path loss on the coverage performance of UAV communications. A tractable UAV model with three-dimensional (3D) static blockage was presented in [26] to characterize the coverage. The work in [27] and [28] analyzed the coverage performance of UAV-enabled cellular networks. Meanwhile, [29] considered the coverage performance of vertical heterogeneous networks (VHetNets). The authors in [30] proposed a multi-tier UAV network, where the positions of UAVs in each layer obey a HPPP. For the clustered distribution scenarios, the coverage probability was studied in [8] and [31], respectively, where the cluster center was modeled as a HPPP. For mmWave UAV networks, the impacts of UAV density, height, and antenna elements, on the coverage performance were discussed in [32] by considering static blockage. In addition, there has been increased attention to the use of finite HPPP (FHPPP) for modeling the positions of BSs in finite areas [33]–[35].

Even though HPPP/FHPPP has been widely used to model the position of UAVs, it is not well suited for some scenarios, especially when deploying a fixed number of UAVs for typical missions. In such cases, BPPs are suitable models to represent the location of UAVs. [36] was the first work to model the UAV networks based on BPP, and [37] studied the outage probability of UAV network based on BPP. However, the results of [36], [37] were obtained conditioned on the line-of-sight (LoS) paths, overlooking the effects of the NLoS portion. Considering the combined impacts of LoS/NLoS components due to static obstacles, a probabilistic channel model was introduced in [22] to study the coverage probability of UAV-assisted network. [38] performed a similar analysis by combining the trajectory of UAVs. Based on the LoS/NLoS model, the coverage performance of VHetNets was studied in [39]. Considering mmWave UAV communications, the authors in [40] evaluated the coverage probability of a large-scale hybrid aerial-terrestrial network, where a BPP is used to generate the positions of UAVs. Recently, a tractable model for multiple-swarm mmWave UAV communications was developed in [7].

While existing studies provide valuable insights, certain research gaps persist regarding the coverage performance of air-to-ground mmWave UAV networks, mainly reflected in two aspects: 1) the blockage effects has not been fully considered, especially the human blockages; 2) the spatial distribution of UAVs has not been adequately characterized, especially the disparities between FHPPP and BPP. The main difference between FHPPP and BPP lies in the distribution of the number of UAVs. However, as more UAVs are deployed, both models tend to exhibit similar conclusion [41]. It is necessary to conduct a uniform analysis of the system performance under these two models to obtain distribution models suitable for networks with varying numbers of UAVs, leading to more effective results. However, theoretical research in this area is lacking although both models are widely used. Therefore, we aimed to examine how various types of mmWave blockages and UAV distribution models influence the coverage performance. To achieve this, we analyze the coverage probability by jointly considering static, dynamic and self blockages, and incorporate these two distribution modes. Additionally, we introduce an average LoS/NLoS probability model and analyze the average path loss to better reflect the effects arising from various blockages. Our previous research [42] focused on the impact of user location changes on coverage performance under the FHPPP model and excludes self-blockage. Consequently, it fell short in evaluating the effects of various mmWave blockages and UAV distribution models on system performance. Further investigation is required to thoroughly assess the impact of these factors on the system performance.

C. Contributions

Our work differs from the state-of-the-art literature [7], [22], [25]–[30], [32], [34]–[40], in three aspects. First, unlike [22], [25]–[30], [34], [36]–[39] that focused on traditional microwaves, our research focuses on mmWave UAV networks. Second, existing works on the coverage performance of mmWave UAV networks primarily considered static blockage, whether it is for single-swarm [35], multiple-swarm [7], or hybrid networks [32], [40]. We study the coverage performance of single-swarm mmWave UAV networks while jointly considering multiple types of blockages. Third, the current research lacks a unified framework to investigate the system performance under FHPPP and BPP modeling. Therefore, the main contributions of this paper are:

(1) We develop a general and tractable analytical model to characterize the coverage performance of single-swarm air-to-ground mmWave UAV networks while jointly considering multiple types of blockages. Unlike existing studies that primarily considered static blockage, the static, dynamic, and self blockages on the system performance are jointly considered. Therefore, our results are more general and closer to realistic, which will provide more accurate and in-depth insights into the parameter design of air-to-ground mmWave UAV networks.

(2) To provide more design guidelines for UAV networks, we treat BPP as a special case of FHPPP and investigate the coverage performance under both models. We first calculate the distributions of distances from a typical user equipment (UE) to its serving and interfering UAVs, along with the Laplace transform of interference for FHPPP modeled UAVs. Based on these, we derive a tractable expression for the coverage probability. Then, we extend the analysis to scenarios with BPP modeled UAVs. Additionally, we conduct an analysis of the average path loss to further reflect the effects arising from various blockages. To our best knowledge, this is the first work to study the system performance of mmWave UAV networks under different UAV distribution models and blockages.

(3) We validate the above results through Monte Carlo simulations, and the results show that: 1) mmWave blockages significantly impacts the performance of mmWave UAV networks. Particularly, static blockage and self-blockage exert predominant influence on the coverage probability, average LoS probability, and average path loss for UAVs at relatively low and high altitudes, respectively, while dynamic blockage cannot be ignored, especially when UAVs operate at lower heights and buildings are sparsely distributed; 2) to avoid self-blockage, the UAV should be sufficiently high. The required height is proportional to the two-dimensional (2D) distance of the UAV-UE link and increases as the distance between the

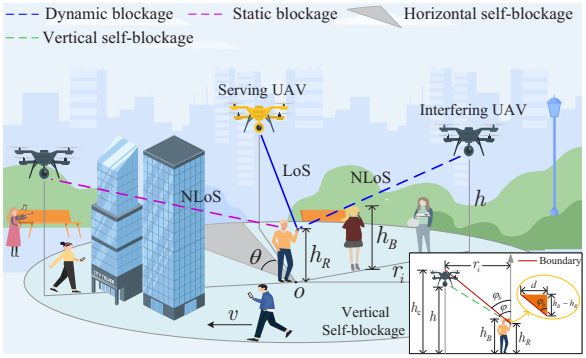

Fig. 1. The system model, where the UE is served by its nearest UAV, buildings, moving humans, and the user himself can potentially block UAV-UE links. Particularly, the vertical self-blockage zone is defined by the area represented by the elevation angle $\varphi(\varphi > \varphi_b)$ between the UAV and the UE.

user and UE decreases; 3) BPP is more suitable for deploying a fixed number of UAVs to cover a small-scale area, while FHPPP is preferable for large-scale deployments; 4) there exist optimal parameters that maximize the system performance, which helps in designing key parameters such as UAVs height.

II. System Model

As illustrated in Fig. 1, we consider mmWave-based UAVs as aerial BSs for ground users. The UAVs are distributed uniformly over a disk $D(o,R)$ with center o and radius R, and hover at the same height h. Following [26], [28], [32], [34], [35], we select the UE at the origin as the typical UE, with its position denoted as $(0,0,h_R)$, where h_R represents its height, and the UE will connect to the nearest UAV.

A. UAV Models

When modeling UAVs, the following two-fold factors are considered: 1) in real-world deployments, it is not uncommon to allow UAVs to fly from one area to another to perform typical missions [7]. This results in a significant variation in the number of UAVs within the considered area, as the number of UAVs fluctuates randomly. Additionally, for large-scale deployments, determining the specific number of UAVs required can be a challenging task; 2) in others, a fixed number of UAVs is employed to cover a given area. As a result, the spatial distribution of UAV locations is assumed separately as:

1) FHPPP modeled UAVs: We assume that the positions of UAVs on the plane follow a FHPPP of parameter λ_T. Thus, the distribution of the number of UAVs N within the disk $D(o,R)$ follows a Poisson distributed with parameter $\lambda_T \pi R^2$, i.e., $\mathbb{P}_N(n) = \frac{[\lambda_T \pi R^2]^n}{n!} \exp\left(-\lambda_T \pi R^2\right)$. Moreover, the probability density function (PDF) of the 2D distance R_i, $i = 1, \cdots, N$ between the i-th UAV and the typical UE is independently and identically distributed (i.i.d.) with distribution [12], [18]

$$f_{R_i}(r_i) = \frac{2r_i}{R^2}; 0 < r_i \leq R, \forall i = 1, \cdots, N. \tag{1}$$

2) BPP modeled UAVs: We assume that the positions of UAVs follow a uniform BPP. Therefore, a fixed number of N UAVs are i.i.d. within the disk $D(o,R)$. The distribution of the distance from the typical UE to UAV is the same as (1).

B. Blockage Models

1) Static Blockage: Following [43], we adopt a probabilistic blockage model to describe the static blockage and define an indicative random variable L_i^{s} to indicate that the i-th UAV-UE link is not blocked by buildings. Then, the non-blockage probability of the link conditioned on h and r_i is given by

$$\mathbb{P}(L_i^{\mathrm{s}}|h, r_i) = \frac{1}{1 + a\exp\left(-b(\arctan(\frac{h-h_R}{r_i})\frac{180}{\pi} - a)\right)}, \tag{2}$$

where a and b are the parameters related to the environment. (2) can be used to various scenarios by setting different a and b, e.g., $(a,b) = (6.7309, 0.4434)$, $(a,b) = (9.6117, 0.1581)$ and $(a,b) = (12.0810, 0.1139)$ correspond to the scenarios of suburban, urban, and dense urban, respectively [43].

2) Dynamic Blockage: We assume humans of height h_B are distributed throughout the disk, forming a FHPPP of density λ_B. These humans move randomly at speed v. The dynamic blockage of link can be treated as an exponential on-off process, characterized by blocking and non-blocking parameters η_i and ω, respectively [12], [18]. We define L_i^{d} to indicate that humans do not block the i-th link, and then,

$$\mathbb{P}(L_i^{\mathrm{d}}|h, r_i) = \frac{\omega}{\eta_i + \omega} = \frac{\omega(h - h_R)}{\rho r_i + \omega(h - h_R)}, \tag{3}$$

where $\rho = 2\lambda_B v(h_B - h_R)/\pi$, $\eta_i = \rho r_i/(h - h_R)$, and ω can be simplified to a constant [12].

3) Self-Blockage: We consider a 3D self-blockage model, as shown in Fig. 1, where self-blockage occurs if and only if the UAV falls within both horizontal and vertical self-blockage zones. The horizontal self-blockage zone is denoted as a sector of disk $D(o,R)$ making an angle θ behind the UE [12]. The vertical self-blockage zone is denoted by the area represented by the elevation angle $\varphi(\varphi > \varphi_b)$ [15]. We define L_i^{sel} to indicate that the i-th link is not self-blocked. Then, we have

Lemma 1. *The conditional probability of the i-th UAV-UE link without self-blockage can be expressed as*

$$\mathbb{P}(L_i^{\mathrm{sel}}|h) = 1 - \frac{\theta}{2\pi}\left(1 - \frac{d^2}{R^2}\frac{(h - h_R)^2}{(h_B - h_R)^2}\right). \tag{4}$$

Proof. The probability of the UAV falling into the horizontal self-blockage zone is obviously equal to $\frac{\theta}{2\pi}$ [12], and only when the height h of the UAV is lower than the height $h_{\mathrm{c}} = h_R + \frac{r_i}{\tan\varphi_b}$ of the boundary line, i.e., $\varphi > \varphi_b$, the UAV is in the vertical self-blockage zone, where $\varphi_b = \arctan\frac{d}{h_B - h_R}$ and d denotes the horizontal distance between the user and the UE [15]. In this way, the probability of the UAV falling into the vertical self-blockage zone can be calculated as $\mathbb{P}(\varphi > \varphi_b) = \mathbb{P}(\arctan\frac{r_i}{h - h_R} > \arctan\frac{d}{h_B - h_R}) = \mathbb{P}(r_i > \frac{d(h-h_R)}{h_B - h_R})$, where the last step follows from the fact that $\arctan(\cdot)$ is an increasing function. Moreover, according to (1), we can get $\mathbb{P}(r_i > \frac{d(h-h_R)}{h_B - h_R}) = 1 - \int_0^{\frac{d(h-h_R)}{h_B - h_R}} \frac{2r_i}{R^2}\mathrm{d}r_i = 1 - \frac{d^2}{R^2}\frac{(h-h_R)^2}{(h_B - h_R)^2}$. Therefore, $\mathbb{P}(L_i^{\mathrm{sel}}|h)$ can be obtained as shown in (4). □

C. Channel and Antenna Models

1) Large-scale Path Loss Model: Since UAV-UE links can be either LoS or NLoS, the large-scale path loss of the i-th UAV-UE link is represented by a discrete random variable

$\ell_k(h, r_i)$, where $k \in \{\mathrm{L}, \mathrm{N}\}$ denotes the LoS (L) or NLoS (N) case. The large-scale path loss can be expressed as [7]

$$\ell_k(h, r_i) = \begin{cases} \left(\sqrt{r_i^2 + (h - h_R)^2}\right)^{-\alpha_{\mathrm{L}}} & \text{w.p.} \quad \mathbb{P}_{\mathrm{L}}(h, r_i), \\ \left(\sqrt{r_i^2 + (h - h_R)^2}\right)^{-\alpha_{\mathrm{N}}} & \text{w.p.} \quad \mathbb{P}_{\mathrm{N}}(h, r_i), \end{cases} \tag{5}$$

where α_{L} and α_{N} represent the path loss parameter for LoS and NLoS link, respectively.

2) Small-scale Fading Model: We employ a Nakagami fading since it is a commonly used fading model that can accurately represent various channel environments [44]. Therefore, the small-scale fading gain, denoted as $\zeta_k, k \in \{\mathrm{L}, \mathrm{N}\}$ follows a Gamma distribution with shape and scale factor of m_k and $1/m_k$, respectively [7]. The PDF of ζ_k is expressed as

$$f_{\zeta_k}(\zeta_k) = \frac{m_k^{m_k} \zeta_k^{m_k - 1}}{\Gamma(m_k)} \exp\left(-m_k \zeta_k\right), k \in \{\mathrm{L}, \mathrm{N}\}, \tag{6}$$

where $\Gamma(\cdot)$ denotes the Gamma function.

3) Antenna Model: We assume that each UAV is mounted with a uniform planar square antenna array (UPA) and the UE has a single antenna. For tractability, the sector antenna pattern mentioned in [7], [45] is adopted, which can provide the main lobe gain G_{m} within half power beam width (θ_a in the azimuth plane and θ_e in the elevation plane) and the side lobe gain G_{s} in other directions, above, $\theta_a = \theta_e = \frac{\sqrt{3}}{\sqrt{M}}$ for a UPA with M antenna elements, G_{m} and G_{s} are given as

$$G_{\mathrm{m}} = M \ \text{ and } \ G_{\mathrm{s}} = \frac{\sqrt{M} - \frac{\sqrt{3}}{2\pi} M \sin(\frac{\sqrt{3}}{2\sqrt{M}})}{\sqrt{M} - \frac{\sqrt{3}}{2\pi} \sin(\frac{\sqrt{3}}{2\sqrt{M}})}, \tag{7}$$

respectively. Let us further assume that the UE and its serving UAV will adjust their antenna directions to perfectly align with each other to achieve the antenna gain G_{m}. For interfering UAVs, we assume that the antenna gain $G_u, u \in \{\mathrm{m}, \mathrm{s}\}$ of any UAV-UE link is a random variable as [7]

$$G_u = \begin{cases} G_{\mathrm{m}} & \text{w.p.} \quad \mathbb{P}_{\mathrm{m}} = \frac{\theta_a}{2\pi} \frac{\theta_e}{\pi/2}, \\ G_{\mathrm{s}} & \text{w.p.} \quad \mathbb{P}_{\mathrm{s}} = 1 - \frac{\theta_a}{2\pi} \frac{\theta_e}{\pi/2}, \end{cases} \tag{8}$$

where $\mathbb{P}_u, u \in \{\mathrm{m}, \mathrm{s}\}$ represents the probability that G_u occurs. Under the above settings and assuming that the horizontal distance between the typical UE and its serving UAV is r_c, the SINR at the typical UE can be expressed as

$$\mathrm{SINR} = \frac{P_t G_{\mathrm{m}} \zeta_k \ell_k(h, r_c)}{N_0 + \sum_{j \in \mathcal{I}} P_t G_u \zeta_k \ell_k(h, r_j)}, \tag{9}$$

where P_t denotes the transmit power of UAVs, N_0 denotes the noise power, and $\mathcal{I}$ represents the set of all interfering UAVs.

III. Analysis of average LoS/NLoS Probability

This section employs an average LoS/NLoS probability model and conduct an analysis on the average path loss of UAV-UE link. The primary objective is to provide insight into the influence of various types of mmWave blockages on the performance of air-to-ground mmWave UAV communications.

According to Section II-B, the LoS probability $\mathbb{P}_{\mathrm{L}}(h, r_i)$ of the i-th UAV-UE link can first be expressed as follows

$$\mathbb{P}_{\mathrm{L}}(h, r_i) = \mathbb{P}(L_i^{\mathrm{s}} | h, r_i) \mathbb{P}(L_i^{\mathrm{d}} | h, r_i) \mathbb{P}(L_i^{\mathrm{sel}} | h), \tag{10}$$

and the NLoS probability is $\mathbb{P}_{\mathrm{N}}(h, r_i) = 1 - \mathbb{P}_{\mathrm{L}}(h, r_i)$. In this case, the average LoS probability can be calculated as follows

$$\mathbb{P}_{\mathrm{AL}} = \int_0^R \mathbb{P}_{\mathrm{L}}(h, r_i) f_{R_i}(r_i) \mathrm{d}r_i, \tag{11}$$

where $f_{R_i}(r_i)$ is given in (1). The average NLoS probability can be denoted as $\mathbb{P}_{\mathrm{AN}} = 1 - \mathbb{P}_{\mathrm{AL}}$. Particularly, in the specific case of open areas without buildings, (10) and (11) can be simplified by setting $\mathbb{P}(L_i^{\mathrm{s}} | h, r_i) = 1$. Similarly, in the situation without moving blockers or self-blockage, (10) and (11) can be simplified by setting $\mathbb{P}(L_i^{\mathrm{d}} | h, r_i)$ and $\mathbb{P}(L_i^{\mathrm{sel}} | h)$ equal to 1, respectively. Therefore, the blockage we considered is more practical and general. Additionally, here we focus more on the blockage of the link between the UE and the serving UAV, i.e., the average LoS/NLoS probability of the serving link. Consequently, next, we will first focus on deriving the PDF of the 2D distance of the serving link.

A. Analysis of Distance Distributions

We refer to the 2D distance from the UE to its serving UAV as the serving distance, and define R_{p} and R_{b} as the serving distance when the locations of UAVs follow the FHPPP and BPP, respectively. Then, we can get the following Lemmas.

Lemma 2. *When the locations of UAVs follow a FHPPP, the PDF of the serving distance R_{p} is given by*

$$f_{R_{\mathrm{p}}}(r_{\mathrm{p}}) = 2\pi \lambda_T r_{\mathrm{p}} \exp\left(-\lambda_T \pi r_{\mathrm{p}}^2\right), 0 \le r_{\mathrm{p}} \le R. \tag{12}$$

Proof. To obtain the PDF of the serving distance R_{p}, we first calculate the cumulative distribution function (CDF) of R_{p}, denoted as $F_{R_{\mathrm{p}}}(r_{\mathrm{p}}) = \mathbb{P}(R_{\mathrm{p}} \le r_{\mathrm{p}})$. Since the UE communicates with the nearest UAV, the serving distance is equal to r_{p} if and only if there are no other UAVs closer than r_{p}. In other words, $\mathbb{P}(R_{\mathrm{p}} \le r_{\mathrm{p}})$ also indicates the probability of having at least one UAV located within the disk $D(o, r_{\mathrm{p}})$. Since the locations of UAVs on the plane are modeled as a FHPPP, the number N_{p} of UAVs in the disk $D(o, r_{\mathrm{p}})$ follows a Poisson distribution, i.e., $\mathbb{P}_{N_{\mathrm{p}}}(n_{\mathrm{p}}) = \frac{[\lambda_T \pi r_{\mathrm{p}}^2]^{n_{\mathrm{p}}}}{n_{\mathrm{p}}!} \exp\left(-\lambda_T \pi r_{\mathrm{p}}^2\right)$. Given this, we have $F_{R_{\mathrm{p}}}(r_{\mathrm{p}}) = \mathbb{P}(R_{\mathrm{p}} \le r_{\mathrm{p}}) = 1 - \mathbb{P}_{N_{\mathrm{p}}}(0) = 1 - \exp\left(-\lambda_T \pi r_{\mathrm{p}}^2\right)$. Finally, we can obtain the PDF of R_{p} by differentiating $F_{R_{\mathrm{p}}}(r_{\mathrm{p}})$ with respect to r_{p}, as shown in (12). □

Lemma 3. *When the locations of UAVs follow a uniform BPP, the PDF of the serving distance R_{b} is given by*

$$f_{R_{\mathrm{b}}}(r_{\mathrm{b}}) = \frac{2 r_{\mathrm{b}}}{R^2} N \left(1 - \frac{r_{\mathrm{b}}^2}{R^2}\right)^{N-1}, 0 \le r_{\mathrm{b}} \le R. \tag{13}$$

Proof. Let $F_{R_{\mathrm{b}}}(r_{\mathrm{b}})$ denote the CDF of R_{b}. According to the proof of Lemma 2, $F_{R_{\mathrm{b}}}(r_{\mathrm{b}}) = \mathbb{P}(R_{\mathrm{b}} \le r_{\mathrm{b}})$ also means the probability that at least one UAV within the disk $D(o, r_{\mathrm{b}})$. Since the number of UAVs N is fixed, we can derive

$$\begin{aligned} F_{R_{\mathrm{b}}}(r_{\mathrm{b}}) &= 1 - \mathbb{P}(R_1 > r_{\mathrm{b}}, \cdots, R_N > r_{\mathrm{b}}) \\ &= 1 - (1 - \mathbb{P}(R_i \le r_{\mathrm{b}}))^N, \end{aligned} \tag{14}$$

where $\mathbb{P}(R_1 > r_\mathrm{b}, \cdots, R_N > r_\mathrm{b})$ represents the probability of having no UAVs within the disk $D(o, r_\mathrm{b})$. The last step follows from the fact that R_i, $i=1, \cdots, N$, are i.i.d. distributed. Since $\mathbb{P}(R_i \leq r_\mathrm{b})$ is the CDF of R_i, we can use (1) to obtain

$$\mathbb{P}(R_i \leq r_\mathrm{b}) = \int_0^{r_\mathrm{b}} \frac{2r_i}{R^2} \mathrm{d}r_i = \frac{r_\mathrm{b}^2}{R^2}. \tag{15}$$

Substituting (15) into (14) and differentiating (14) with respect to r_b, we can finally get $f_{R_\mathrm{b}}(r_\mathrm{b})$, as shown in (13). □

Finally, by substituting $f_{R_i}(r_i)$ in (11) with $f_{R_c}(r_c), c \in \{\mathrm{p}, \mathrm{b}\}$, we can obtain the average LoS probability $\mathbb{P}_{\mathrm{AL},c}$ of the serving link. In addition, using (5) and (11), we can investigate the average path loss $PL_c, c \in \{\mathrm{p}, \mathrm{b}\}$ of the serving link. The expression for PL_c can be calculated as follows

$$PL_c = \int_0^R \sum_{k \in \{\mathrm{L}, \mathrm{N}\}} \mathbb{P}_k(h, r_c) \ell_k(h, r_c) f_{R_c}(r_c) \mathrm{d}r_c, c \in \{\mathrm{p}, \mathrm{b}\}. \tag{16}$$

According to (11) and (16), we can delve deeper into assessing the impact of various types of blockages on the considered mmWave UAV network. Particularly, the expressions we provided can be applied to various scenarios by flexibly adjusting $\mathbb{P}_\mathrm{L}(h, r_c)$, as detailed in the description of (11). In the subsequent section, we will illustrate the variation trends of $\mathbb{P}_{\mathrm{AL},c}$ and PL_c in various scenarios, thereby demonstrating the necessity of jointly considering multiple types of mmWave blockages. Additionally, intuitively, Lemma 2 and 3 are different. However, for the BPP model we considered, the number N_b of UAVs in the disk $D(o, r_\mathrm{b})$ follows a binomial distribution with parameter r_b^2/R^2, i.e., the probability that there are n_b UAVs in $D(o, r_\mathrm{b})$ is $\mathbb{P}_{N_\mathrm{b}}(n_\mathrm{b}) = \binom{N}{n_\mathrm{b}} \left(\frac{r_\mathrm{b}^2}{R^2}\right)^{n_\mathrm{b}} \left(1 - \frac{r_\mathrm{b}^2}{R^2}\right)^{N - n_\mathrm{b}}$ [24], [41]. In this way, (14) can also be calculated as $F_{R_\mathrm{b}}(r_\mathrm{b}) = 1 - \mathbb{P}_{N_\mathrm{b}}(0)$, which is similar to the calculation of $F_{R_\mathrm{p}}(r_\mathrm{p})$. Furthermore, as N larger, the Poisson distribution and binomial distribution will be consistent [41], i.e., as N increases, Lemma 2 and 3 will become the same, resulting in similar trends and conclusions in terms of system performance under both models. This prompts us to consider the BPP as a special case of the FHPPP to establish a unified analytical framework under these two models, and to explore the system performance under both models for different values of N.

Similarly, we can obtain the PDF of the interfering distance to evaluate the average LoS/NLoS probability of the interfering link. Specifically, since the UE is served by its nearest UAV, given serving distance r_c, $c \in \{\mathrm{p}, \mathrm{b}\}$, interfering UAVs are distributed outside the disk $D(o, r_c)$. We define $\mathcal{I}$ as the set of all interfering UAVs, and $\{R_j\}_{j \in \mathcal{I}}$ as the distances from the UE to its interfering UAVs, hereinafter referred to as the interfering distance. Then, the PDF of R_j can be obtained.

Lemma 4. *Conditioned on the serving distance r_c, $c \in \{\mathrm{p}, \mathrm{b}\}$, the PDF of the interfering distance R_j from the typical UE to its j-th interfering UAV is given by*

$$f_{R_j}(r_j | r_c) = \frac{2r_j}{R^2 - r_c^2}, r_c \leq r_j \leq R. \tag{17}$$

Proof. First, we calculate the conditional CDF of R_j, denoted as $F_{R_j}(r_j | r_c)$. As mentioned above, conditioned on $r_c, c \in \{\mathrm{p}, \mathrm{b}\}$, the interfering UAVs are distributed outside the disk $D(o, r_c)$. Therefore, we have $r_c \leq r_j \leq R$, and then, $F_{R_j}(r_j | r_c) = \mathbb{P}(R_j \leq r_j)$ can be calculated as

$$F_{R_j}(r_j | r_c) = \frac{\int_{r_c}^{r_j} \frac{2r_j}{R^2} \mathrm{d}r_j}{\int_{r_c}^{R} \frac{2r_j}{R^2} \mathrm{d}r_j} = \frac{r_j^2 - r_c^2}{R^2 - r_c^2}. \tag{18}$$

Finally, the PDF of R_j, denoted as $f_{R_j}(r_j | r_c)$ can be obtained as $f_{R_j}(r_j | r_c) = \frac{\partial F_{R_j}(r_j | r_c)}{\partial r_j}$, as shown in (17). □

By substituting $f_{R_i}(r_i)$ in (11) with $f_{R_j}(r_j | r_c), c \in \{\mathrm{p}, \mathrm{b}\}$, we can obtain the average LoS probability of the interfering links under the FHPPP and BPP models, respectively.

IV. Analysis of Coverage Probability

This section focus on evaluating the coverage probability of air-to-ground mmWave UAV communication by jointly considering multiple types of blockages. The coverage probability, denoted as $\mathbb{P}_\mathrm{cov}$, is defined as follows

$$\mathbb{P}_\mathrm{cov} \triangleq \mathbb{P}\left(\mathrm{SINR} > T\right), \tag{19}$$

which represents the probability that the SINR is larger than a given threshold T. Next, we first provide the Laplace transform of the interference signal, which is a key intermediate step in obtaining the tractable expression of $\mathbb{P}_\mathrm{cov}$.

A. Analysis of Interference Power

According to (9), the interference signal I is given by

$$I = \sum_{j=1}^{N_\mathrm{a}} P_t G_u \zeta_k \ell_k(h, r_j), \tag{20}$$

where $k \in \{\mathrm{L}, \mathrm{N}\}, u \in \{\mathrm{m}, \mathrm{s}\}$, $N_\mathrm{a} = |\mathcal{I}|$ denotes the number of interfering UAVs. Then, the Laplace transform of I in our cases is given by Theorem 1 and Corollary 1, respectively.

Theorem 1. *For the case of FHPPP modeled UAVs, conditioned on the serving distance r_p, the Laplace transform of aggregate interference I can be expressed as*

$$\mathcal{L}_I(s | r_\mathrm{p}) = \exp\Bigg(- 2\pi\lambda_T \int_{r_\mathrm{p}}^R r_j \Big(1 - \mathbb{E}_\Psi\left[\exp\left(-sP_t G_u \zeta_k \ell_k(h, r_j)\right)\right]\Big) \mathrm{d}r_j \Bigg), \tag{21}$$

where $\mathbb{E}_\Psi\left[\exp\left(-sP_t G_u \zeta_k \ell_k(h, r_j)\right)\right] = \sum_{k \in \{\mathrm{L}, \mathrm{N}\}} \mathbb{P}_k(h, r_j) \times \sum_{u \in \{\mathrm{m}, \mathrm{s}\}} \mathbb{P}_u \left(\frac{m_k}{m_k + sP_t G_u \ell_k(h, r_j)} \right)^{m_k}$.

Proof. The proof is given in Appendix A. □

Theorem 1 describes the statistical properties of interference and plays a vital role in the coverage analysis below. It is evident that parameters such as link blockage and antenna configuration will affect the interference signal and thus affect the coverage performance. After all, it is necessary to evaluate the impact of various parameters on establishing reliable

communications in terms of achieving maximum coverage. Similar to Theorem 1, we obtain Corollary 1 as follows.

Corollary 1. *For the case of BPP modeled UAVs, conditioned on the serving distance $r_{\rm b}$, the Laplace transform of aggregate interference I can be expressed as*

$$\mathcal{L}_I(s|r_{\rm b})=\Bigg[\frac{2}{R^2-r_{\rm b}^2}\int_{r_b}^{R} r_j \sum_{k\in\{\rm L,N\}}\mathbb{P}_k(h,r_j)\sum_{u\in\{\rm m,s\}}\mathbb{P}_u \times\left(\frac{m_k}{m_k+sP_tG_u\ell_k(h,r_j)}\right)^{m_k}{\rm d}r_j\Bigg]^{N-1}. \quad (22)$$

Proof. The proof is given in Appendix B. □

Based on the distance distributions and the Laplace transform of interference, we can derive the coverage probability to evaluate the coverage performance of the considered communication system. The specific details are given as follows.

B. Analysis of Coverage Probability

According to (19), (12) and (13), the coverage probability averaged over the distribution of the serving distance can be represented as follows

$$\mathbb{P}_{\rm cov}=\int_0^R \mathbb{P}\left({\rm SINR}>T|r_c\right) f_{R_c}(r_c){\rm d}r_c, \quad (23)$$

and for convenience of express, we denote $\mathbb{P}_{\rm cov,p}$ and $\mathbb{P}_{\rm cov,b}$ as the coverage probability for the case of FHPPP modeled and BPP modeled UAVs, respectively. Subsequently, the tractable expressions of $\mathbb{P}_{\rm cov,p}$ and $\mathbb{P}_{\rm cov,b}$ are obtained as shown in Theorem 2 and Corollary 2, respectively.

Theorem 2. *For the case of FHPPP modeled UAVs, the coverage probability $\mathbb{P}_{\rm cov,p}$ can be approximated as*

$$\mathbb{P}_{\rm cov,p}\approx 2\pi\lambda_T\int_0^R\sum_{k\in\{\rm L,N\}}\mathbb{P}_k(h,r_{\rm p})\sum_{m=1}^{m_k}(-1)^{m+1}C_{m_k}^m \times\exp\left(\frac{-m\xi_kTN_0}{P_tG_{\rm m}\ell_k(h,r_{\rm p})}\right)\exp\left(-\lambda_T\pi r_{\rm p}^2\right) \times\mathcal{L}_I\left(\frac{m\xi_kT}{P_tG_{\rm m}\ell_k(h,r_{\rm p})}\middle|r_{\rm p}\right)r_{\rm p}{\rm d}r_{\rm p}, \quad (24)$$

where $\mathbb{P}_{\rm L}(h,r_{\rm p})$ is the LoS probability of the serving link, $\mathbb{P}_{\rm N}(h,r_{\rm p})=1-\mathbb{P}_{\rm L}(h,r_{\rm p})$, $\xi_k=m_k(m_k!)^{-1/m_k}$, $\ell_k(h,r_{\rm p})=\left(\sqrt{r_{\rm p}^2+(h-h_R)^2}\right)^{-\alpha_k}$, and $\mathcal{L}_I\left(\frac{m\xi_kT}{P_tG_{\rm m}\ell_k(h,r_{\rm p})}\middle|r_{\rm p}\right)$ can be obtained according to Theorem 1.

Proof. The proof is given in Appendix C. □

According to Theorem 2, we can evaluate the effects of key parameters such as UAVs height, density, mmWave blockages on the coverage, and reveal hidden trade-offs in designing UAV networks. Since the LoS probability in this paper jointly considers multiple types of blockages, the evaluation of the performance is more closer to reality and general, specifically refer to the description of (11). When the positions of UAVs follow a BPP, the converge probability is obtained as follows.

Corollary 2. *For the case of BPP modeled UAVs, the coverage probability $\mathbb{P}_{\rm cov,b}$ can be approximated as*

$$\mathbb{P}_{\rm cov,b}\approx\frac{2N}{R^2}\int_0^R\sum_{k\in\{\rm L,N\}}\mathbb{P}_k(h,r_{\rm b})\sum_{m=1}^{m_k}(-1)^{m+1}C_{m_k}^m \times\exp\left(\frac{-m\xi_kTN_0}{P_tG_{\rm m}\ell_k(h,r_{\rm b})}\right)\left(1-\frac{r_b^2}{R^2}\right)^{N-1} \times\mathcal{L}_I\left(\frac{m\xi_kT}{P_tG_{\rm m}\ell_k(h,r_{\rm b})}\middle|r_{\rm b}\right)r_{\rm b}{\rm d}r_{\rm b}. \quad (25)$$

Proof. The proof is given in Appendix D. □

Considering a special situation where the serving UAV is hovering right above the UE, we can obtain Corollary 3.

Corollary 3. *Under the special situation, the coverage probability $\mathbb{P}_{\rm cov,p}$ and $\mathbb{P}_{\rm cov,b}$ can be uniformly represented as*

$$\mathbb{P}_{\rm cov}\approx\sum_{m=1}^{m_{\rm L}}(-1)^{m+1}C_{m_{\rm L}}^m\exp\left(\frac{-m\xi_{\rm L}TN_0}{P_tG_{\rm m}\ell_{\rm L}(h,0)}\right) \times\mathcal{L}_I\left(\frac{m\xi_{\rm L}T}{P_tG_{\rm m}\ell_{\rm L}(h,0)}\middle|r_c=0\right), c\in\{\rm p,b\}. \quad (26)$$

Proof. It is clear that the serving distance is $r_c=0, c\in\{\rm p,b\}$ and the serving link is LoS, i.e., $\mathbb{P}_k(h,r_c)=\mathbb{P}_{\rm L}(h,0)=1$ when the serving UAV is hovering directly above the UE. Therefore, (24) and (25) are simplified as shown in (26). □

Algorithm 1 Optimal UAVs Height Search Based on PSO

Initialize: Generate the initial height $\{h_j^0\}_{j=1}^J$ under the constraints of (27a) and initial velocity $\{V_j\}_{j=1}^J$ with uniform distribution in the range of $[H_{\min},H_{\max}]$, calculate the fitness $f(h_j^0)$ for each particle according to (24) or (25), and set $f^*(h_j^*)=f(h_j^0)$, $f^{\triangle}(h^{\triangle})=\max_j f^*(h_j^*)$.

Repeat:

1: **for** each particle $j\in[1,J]$ **do**
2: update V_j and h_j using (28) and (29), respectively.
3: if $f(h_j)>f^*(h_j^*)$
4: Update individual best position: $h_j^*\leftarrow h_j$.
5: **for** each particle $j\in[1,J]$ **do**
6: if $f^*(h_j^*)>f^{\triangle}(h^{\triangle})$
7: update global best position: $h^{\triangle}\leftarrow h_j^*$.

Until: UAVs height do not change or the procedure reaches the maximum number of iterations.

Based on the derived expression, we can demonstrate the variation trends of the coverage probability under various design parameters to identify the optimal parameters, such as the optimal UAVs height, that maximize the coverage performance. Additionally, we can explore the optimal parameters through numerical optimization algorithms. The problem of maximizing the coverage probability can be formulated as

$$\max_h\ f(h)=\mathbb{P}_{\rm cov} \quad (27)$$

$$\text{s.t. } H_{\min}\le h\le H_{\max}, \quad (27a)$$

TABLE I
SIMULATION PARAMETER VALUES

Parameter	Description	Value
$\alpha_{\mathrm{L}}/\alpha_{\mathrm{N}}$	Path loss parameter for LoS/NLoS link	2/4 [8]
$m_{\mathrm{L}}/m_{\mathrm{N}}$	Fading parameter for LoS/NLoS link	3/2 [8]
h_R/h_B	Height of the UE/humans	1.4/1.8 m [12]
h	Height of UAVs	50 m
v	Velocity of the moving humans	1 m/s [12]
θ	Horizontal self-blockage angle	$\pi/3$ [12]
d	Horizontal distance from user to UE	0.15 m [15]
λ_B	Density of the moving blockers	0.01 bl/m^2
λ_T	PPP modeled density of UAVs	2×10^{-4}/m^2
M	Number of antenna elements	16
R	Communication range of UAVs	100 m
T	Threshold of SINR	3 dB
P_t	Transmit power of UAVs	20 dBm [7]
N_0	Noise power	-110 dBm

where (27a) confines the search region of UAVs height. Subsequently, we develop a particle swarm optimization (PSO)-based algorithm to solve (27) due to its fast computation speed, high efficiency, and fewer parameters [46], [47].

We assume there are J particles, where each particle represents a candidate solution of the optimal height, denoted as $\{h_j\}_{j=1}^{J}$ for convenience. Each particle also has a velocity V_j to update its height. Therefore, we first generate a set $\{h_j^0\}_{j=1}^{J}$ to represent the initial UAVs height. Then, random initial velocity $\{V_j\}_{j=1}^{J}$ with a uniform distribution over $[H_{\min}, H_{\max}]$ are generated. The fitness of each particle at current height can be evaluated by (24) or (25), depending on the distribution of UAVs. All particles store their individual best heights $\{h_j^*\}_{j=1}^{J}$ that achieve optimum fitness values so far. Subsequently, the global optimal fitness can be obtained through the global optimal height $\{h^{\triangle}\}_{j=1}^{J}$ of all the particles so for. In each iteration, the velocity is refined as follows [46]

$$\begin{aligned} V_j \leftarrow \varpi V_j &+ \xi_1\eta_1\left(h_j^* - h_j\right) \\ &+ \xi_2\eta_2\left(h^{\triangle} - h_j\right), j = 1, \cdots, J, \end{aligned} \tag{28}$$

where ϖ is the inertia factor, ξ_1 and ξ_2 are the individual and social learning factors. η_1 and η_2 are uniformly distributed variables within $[0, 1]$. The height is updated by

$$h_j \leftarrow h_j + V_j, j = 1, \cdots, J. \tag{29}$$

Details of the PSO algorithm are provided in Algorithm 1. This algorithm can be applied to optimize other parameters by replacing the height with the desired optimized parameter.

V. SIMULATION AND DISCUSSION

This section performs extensive Monte Carlo simulations to validate the theoretical results. Unless stated otherwise, Table I presents the values for some typical simulation parameters, and the urban scenario is considered.

A. Analysis of coverage probability for FHPPP modeled UAVs

Fig. 2 shows the coverage probability $\mathbb{P}_{\mathrm{cov,p}}$ versus the height h of UAVs for three different scenarios and SINR thresholds T. The difference between the scenarios lies in a and b, as explained in subsection II-B. As expected, $\mathbb{P}_{\mathrm{cov,p}}$

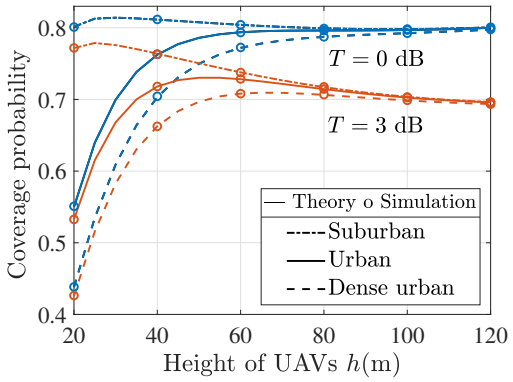

Fig. 2. Coverage probability $\mathbb{P}_{\mathrm{cov,p}}$ versus the height of UAVs h.

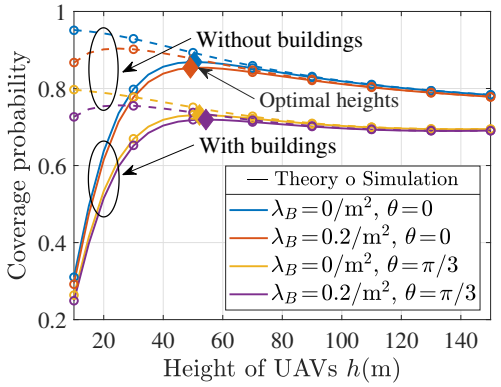

Fig. 3. Comparison of the effects of different types of blockages on $\mathbb{P}_{\mathrm{cov,p}}$. When $\lambda_B = \theta = 0$, $\mathbb{P}_{\mathrm{cov,p}}$ can serve as a benchmark for the coverage probability of terrestrial BSs in the existing work [48], [49]. Additionally, the diamond indicates the optimal UAVs height obtained by Algorithm 1.

decreases as T increases, and there is an optimal h that maximizes $\mathbb{P}_{\mathrm{cov,p}}$, which is due to two factors. On the one hand, increasing h results in an increase in LoS probability $\mathbb{P}_{\mathrm{L}}(h, r_{\mathrm{p}})$, leading to an increase in signal power. On the other hand, increasing h also leads to a longer transmission distance and a significant path loss, even in scenarios with high $\mathbb{P}_{\mathrm{L}}(h, r_{\mathrm{p}})$, thus preventing successful communication. Furthermore, we observe that the optimal h increases with the number of buildings (the number of buildings in urban is higher than that in suburban). Therefore, compared to deploying UAVs in suburban areas, when deploying UAVs in urban areas, we need to place them at relatively high altitudes.

Fig. 3 studies the effects of mmWave blockages on $\mathbb{P}_{\mathrm{cov,p}}$. It is observed that when h is relatively high, $\mathbb{P}_{\mathrm{cov,p}}$ is mainly dominated by self-blockage, while the impact of static and dynamic blockage on the $\mathbb{P}_{\mathrm{cov,p}}$ is negligible. Specifically, the difference in $\mathbb{P}_{\mathrm{cov,p}}$ between urban scene with buildings and open scene without buildings, as well as between scenes with λ_B of 0 and $0.2/\mathrm{m}^2$, can be ignored. However, changes in θ will have a meaningful impact on $\mathbb{P}_{\mathrm{cov,p}}$. The main reason is that at such heights, UAVs can already bypass static and dynamic blockages. However, since the user and the UE are usually very close, the UAV needs to be high enough to bypass self-blockage. In this way, the coverage performance

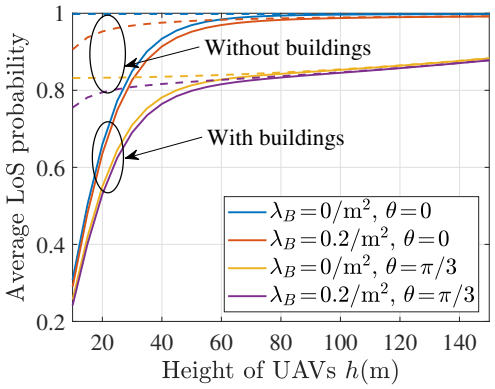

Fig. 4. Average LoS probability $\mathbb{P}_{\mathrm{AL,p}}$ versus the height of UAVs h for different types of blockages (static, dynamic, and self blockages).

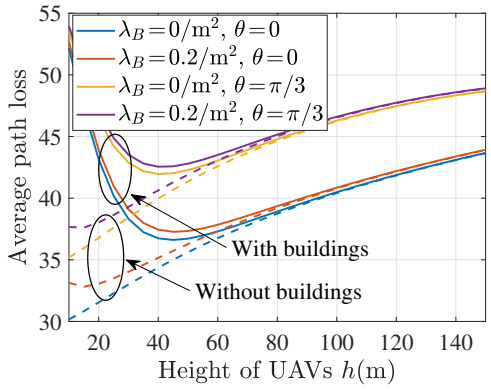

Fig. 5. Average path loss PL_{p} versus the height of UAVs h for different types of blockages (static, dynamic, and self blockages).

is dominated by self-blockage. As detailed below: as shown in Fig. 1, only when h satisfies $h>h_{\mathrm{c}}=h_R+\frac{r_i}{\tan\varphi_b}$, can UAVs bypass vertical self-blockage. Since $\varphi_b = \arctan\frac{d}{h_B-h_R}$, $h_{\mathrm{c}} \approx 1.4+\frac{r_i}{0.37}$ by using Table I. Assuming $r_i = 50$ m, we can get $h_{\mathrm{c}} \approx 137$ m. However, in our considered system, UAVs are uniformly distributed in a disk with radius of 100 m. Therefore, most UAVs need to have a height greater than 137 m to bypass self-blockage. At such height, UAVs can already bypass other blockages since the curves with and without buildings/humans basically coincide when other parameters are consistent if $h>70$ m. For UAVs at relatively low heights, the three blockages will affect the coverage performance, with static blockage having a greater influence than other blockages. This is reasonable since the size of humans is much smaller than that of buildings, so the blockage is mainly caused by buildings, and the coverage performance is mainly affected by static blockage. It is also obvious that $\mathbb{P}_{\mathrm{cov,p}}$ decreases with the increase of λ_B, especially for the case of low UAV heights and sparse or no buildings. This happens because an increase in human blockers leads to a decrease in LoS probability, thereby reducing $\mathbb{P}_{\mathrm{cov,p}}$. All in all, our results indicate that each blockage leads to a deviation in coverage performance. Compared to terrestrial BSs, our solution is also more accurate because existing works on the coverage performance of terrestrial BSs did not consider human blockages [48], [49].

Fig. 3 also illustrates the existence of optimal UAVs deployment height that maximizes the coverage probability. The reasons for this phenomenon can be found in the analysis of Fig. 2. Particularly, the diamond in Fig. 3 represents the optimal height obtained through Algorithm 1 based on PSO, where we assume $\varpi = 0.8$, $\xi_1 = 0.5$, $\xi_2 = 0.2$, and $J = 10$. Obviously, the optimal deployment height of UAVs obtained from theoretical formula (24) and PSO-based algorithm 1 is almost consistent, although they used different methods, which further demonstrates the correctness of our analysis results.

Fig. 4 and 5 illustrate the variation trends of average LoS probability $\mathbb{P}_{\mathrm{AL,p}}$ and path loss PL_{p} with UAVs height h under different blockages conditions, respectively. These visualizations help to further elucidate the influence of diverse blockages on the system performance. First, it is evident from Fig. 4 that $\mathbb{P}_{\mathrm{AL,p}}$ increases with the increase of h but decreases

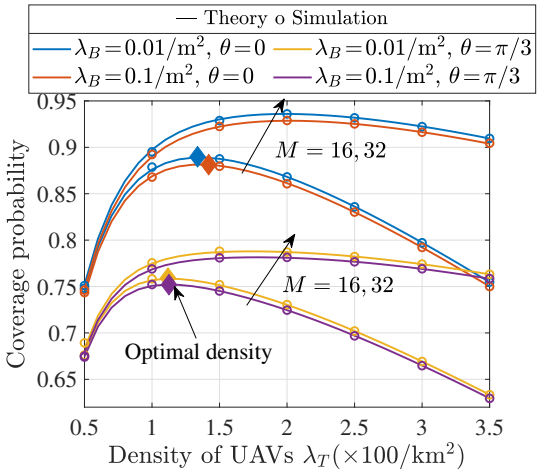

Fig. 6. Coverage probability $\mathbb{P}_{\mathrm{cov,p}}$ versus the density of UAVs λ_T for different blocker densities λ_B and number of antenna elements M. The diamond indicates the optimal density obtained by Algorithm 1 for $M=16$.

with the increase of blockers. Particularly, at greater h, $\mathbb{P}_{\mathrm{AL,p}}$ is predominantly impacted by self-blockage, while the effects of static and dynamic blockages can be negligible. This observation corresponds to the results in Fig. 3 and 5. For a detailed analysis, please refer to Fig. 3. Then, Fig. 5 also demonstrates the presence of an optimal UAVs height that minimizes the average path loss. This phenomenon arises from two primary factors. Firstly, as UAVs height increases, the probability of LoS communication also increases, resulting in a decrease in signal attenuation and reduced PL_{p}. However, elevated heights can lead to excessive transmission distances, causing heightened path loss and subsequently raising PL_{p}. All in all, Fig. 3-5 intuitively reflect the impact of various blockages on mmWave UAV communication system, highlighting the necessity of considering all three types of mmWave blockages simultaneously in the system performance analysis.

Fig. 6 demonstrates the trend of $\mathbb{P}_{\mathrm{cov,p}}$ when varying UAVs density λ_T and antenna elements M. It is clear that there is an optimal density that maximizes $\mathbb{P}_{\mathrm{cov,p}}$ for the following reasons. First, when λ_T is small, UAVs are sparsely distributed, the desired signal power dominates $\mathbb{P}_{\mathrm{cov,p}}$. Therefore, the increase in λ_T will make the distribution of UAVs becomes

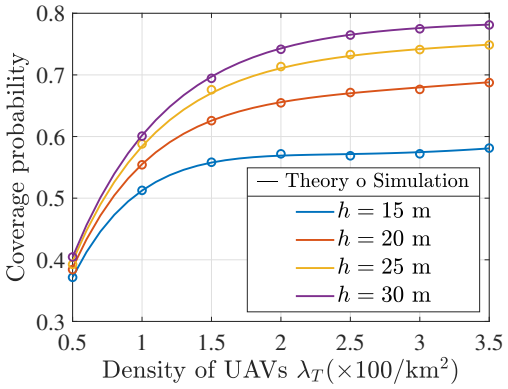

Fig. 7. Coverage probability $\mathbb{P}_{\text{cov,p}}$ versus the density of UAVs λ_T.

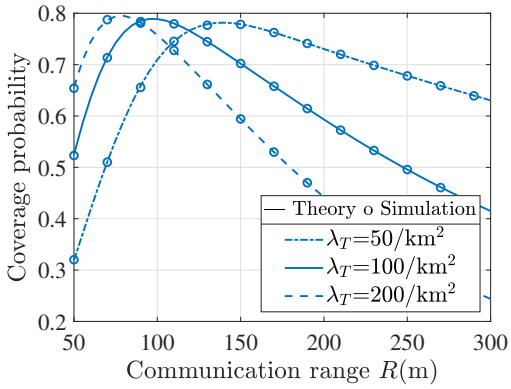

Fig. 8. Coverage probability $\mathbb{P}_{\text{cov,p}}$ versus the communication range of UAVs R.

denser so that the UE will get a better link. However, for larger λ_T, interference becomes the primary limiting factor for $\mathbb{P}_{\text{cov,p}}$, and the increase of λ_T will lead to more interference. Therefore, optimal density exists to maximize $\mathbb{P}_{\text{cov,p}}$. Then, it is observed that when λ_T is large, $\mathbb{P}_{\text{cov,p}}$ increases more obviously with M. This is because interference dominates $\mathbb{P}_{\text{cov,p}}$ at this time, and large antenna arrays are conducive to reducing interference. In addition, Fig. 6 shows that it is possible to perform a trade-off between λ_T and M. For instance, for $\lambda_B = 0.01/\text{m}^2$ and $\theta = \pi/3$, to achieve $\mathbb{P}_{\text{cov,p}} = 0.75$, the required λ_T is $100/\text{km}^2$ when $M = 16$. However, the required λ_T will be significantly (about $80/\text{km}^2$) reduced when $M = 32$. Fig. 6 also presents the optimal UAVs density obtained by Algorithm 1 based on PSO, where we consider $M = 16$. It is evident that the optimal density obtained through Algorithm 1 is almost identical to the results obtained through theoretical formulas. This indicates that the tractable expression for the coverage probability we obtained can effectively demonstrate the trend of the system coverage performance with various deployment parameters and explore the optimal parameters to maximize the coverage performance.

Fig. 7 illustrates the trade-off between the height h and the density λ_T of the UAVs that need to be deployed, where $R = 60$ m. It can be observed from Fig. 7 that by deploying UAVs at a higher height, the required density of UAVs can be reduced without changing the coverage probability $\mathbb{P}_{\text{cov,p}}$. For example, to meet the demand of $\mathbb{P}_{\text{cov,p}} = 0.6$, the minimum UAV density λ_T required is $\lambda_T > 350/\text{km}^2$ when $h = 15$ m. However, the required UAV density can be reduced to $\lambda_T = 100/\text{km}^2$ when the height of UAVs increases to $h = 30$ m. Therefore, increasing the height of UAVs is an effective solution to enhance the coverage performance of the system, which can not only reduce the cost but also simplify the dense network compared to deploying more UAVs.

Fig. 8 shows the impact of the communication range R on $\mathbb{P}_{\text{cov,p}}$. It is evident that there exists an optimal R that maximizes $\mathbb{P}_{\text{cov,p}}$, and this optimal R is affected by the density of UAVs. These are caused by two factors. On the one hand, when R is small, a larger λ_T corresponds to a larger number of UAVs since the number of UAVs follows a Poisson distribution with mean $\lambda_T \pi R^2$. Therefore, increasing λ_T can

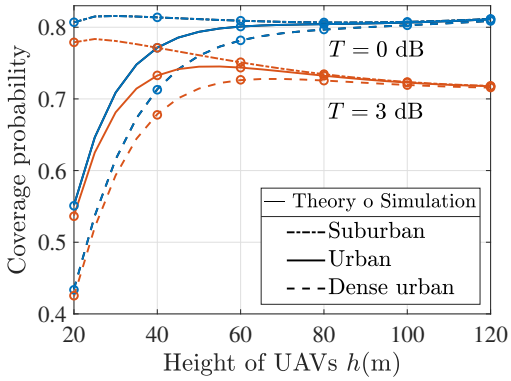

Fig. 9. Coverage probability $\mathbb{P}_{\text{cov,b}}$ versus the height of UAVs h.

increase the average number of UAVs so that the typical UE may get a better communication link to improve the coverage probability. Similarly, a modest increase in R can also improve the coverage probability. However, when R becomes too large, excessive increases in the number of UAVs will result in severe interference. Therefore, at this point, a smaller λ_T helps reduce interference and improve the coverage probability.

B. Analysis of coverage probability for BPP modeled UAVs

Fig. 9 and Fig. 10 illustrate the relationship between the coverage probability $\mathbb{P}_{\text{cov,b}}$ and the height h of UAVs for various parameters. In both figures, it is evident that there exists an optimal h that maximizes $\mathbb{P}_{\text{cov,b}}$. This highlights the crucial role of the height of UAVs as a design parameter in UAV communication systems. By flexibly adjusting the height, better communication quality can be achieved.

Similar to Fig. 2, Fig. 9 shows the impact of the communication scenario and SINR threshold on $\mathbb{P}_{\text{cov,b}}$. It can be seen that $\mathbb{P}_{\text{cov,b}}$ decreases with the increase of T and obstacles. This is reasonable because the increase of T means tighter constraints on the channel quality. The probability of satisfying this requirement decreases as T increases. Similarly, the increase of obstacles will reduce the LoS probability of the link and deteriorate the channel quality and the coverage performance. However, for higher h, $\mathbb{P}_{\text{cov,b}}$ exhibits minimal

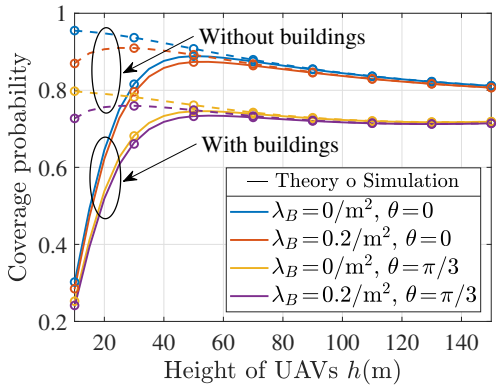

Fig. 10. Comparison of the effects of different types of blockages on $\mathbb{P}_{\mathrm{cov,b}}$. When $\lambda_B = \theta = 0$, $\mathbb{P}_{\mathrm{cov,b}}$ can serve as a benchmark for the coverage probability of a single-warm UAV network mentioned in [7].

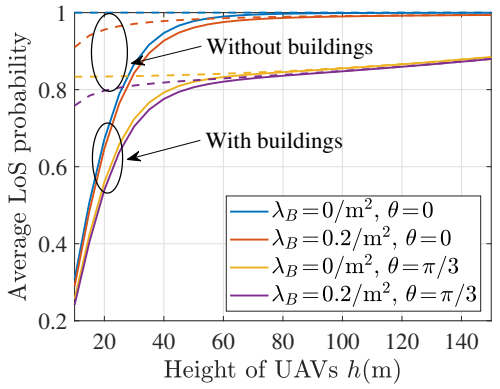

Fig. 11. Average LoS probability $\mathbb{P}_{\mathrm{AL,b}}$ versus the height of UAVs h for different types of blockages (static, dynamic, and self blockages).

change with variations in the environment. This is because at higher heights, $\mathbb{P}_{\mathrm{L}}(h, r_{\mathrm{b}})$ remains high regardless of environmental changes, and the dominant factor influencing $\mathbb{P}_{\mathrm{cov,b}}$ becomes the transmission distance between the UE and UAV.

Fig. 10 plots $\mathbb{P}_{\mathrm{cov,b}}$ as a function of h for various blockages. When $\lambda_B = \theta = 0$, $\mathbb{P}_{\mathrm{cov,b}}$ can be considered as the coverage probability of single-warm UAV network case mentioned in [7], which we use as a benchmark. We compare the coverage performance of our solution against the benchmark. The results indicate that human blockages do indeed affect the performance of such networks, which is expected due to the susceptibility of mmWave to blockages, even human bodies can reduce mmWave signal strength by 20 dB [19]. Therefore, jointly considering multiple types of blockages helps to accurately assess system performance. Specifically, it is clear that $\mathbb{P}_{\mathrm{cov,b}}$ significantly decreases when λ_B and θ are not equal to 0, especially for open-area scenes without buildings. More importantly, misrepresenting the performance can affect the evaluation of key design parameters. For example, in an urban environment with buildings, setting $h \geq 40$ m can achieve the demand of $\mathbb{P}_{\mathrm{cov,b}} \geq 0.8$ when $\theta = 0$ (i.e., without self-blockage). However, self-blockage does exist in practice and it will lead to $\mathbb{P}_{\mathrm{cov,b}} < 0.8$ at the same height. Consequently, to meet the same needs, other parameters such as UAVs

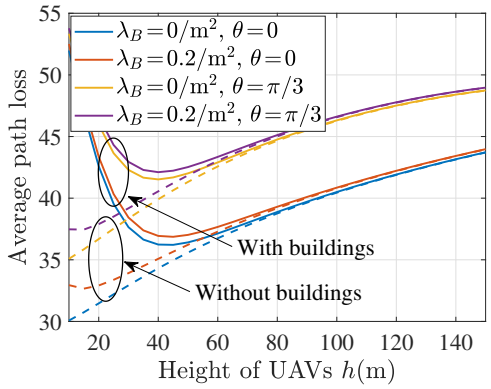

Fig. 12. Average path loss PL_{b} versus the height of UAVs h for different types of blockages (static, dynamic, and self blockages).

density and antenna configuration need to be well-designed. The impact of moving humans is also inevitable. Therefore, analyzing coverage performance by jointly considering the three types of blockages can lead to more accurate results and provide in-depth insights. Fig. 11 and 12 provide additional insights into the impact of mmWave blockages on the system. They depict the trends of this influence on the average LoS probability $\mathbb{P}_{\mathrm{AL},b}$ and path loss PL_{b}. The results are similar to the findings in Fig. 4 and 5, respectively. Particularly, the average LoS probability is primarily influenced by self-blockage when UAVs at higher altitudes. Consequently, PL_{b} during these instances predominantly arises from self-blockage.

It seems that Fig. 9 and 10 have similar trends and conclusions to Fig. 2 and 3, respectively. This is because Fig. 9 and 10 depict $\mathbb{P}_{\mathrm{cov,b}}$ versus h, while Fig. 2 and 3 plot $\mathbb{P}_{\mathrm{cov,p}}$ versus h. $\mathbb{P}_{\mathrm{cov,p}}$ and $\mathbb{P}_{\mathrm{cov,b}}$ are the coverage probabilities under FHPPP and BPP models, respectively. The difference between these two models is that for FHPPP, the number of UAVs N is Poisson distributed, while for BPP, N is fixed, as detailed in Section II. A. For the simulation, the number of UAVs under both models is approximately the same, determined by $\lambda_T \pi R^2 \approx 6$ and $N = 6$, respectively. Hence, $\mathbb{P}_{\mathrm{cov,p}}$ and $\mathbb{P}_{\mathrm{cov,b}}$ may yield similar performance. Similarly, Fig. 4, 5 and Fig. 11, 12 show similar trends and conclusions, respectively.

Fig. 13 demonstrates the impact of the number of UAVs N and of antenna elements M on $\mathbb{P}_{\mathrm{cov,b}}$. It is evident that when N is small, $\mathbb{P}_{\mathrm{cov,b}}$ changes slightly with the increase of M, because the interference is weak at this time. The transmission distance between the UE and the UAV mainly limits $\mathbb{P}_{\mathrm{cov,b}}$. However, when N is large, $\mathbb{P}_{\mathrm{cov,b}}$ increases significantly with the increase of M, because $\mathbb{P}_{\mathrm{cov,b}}$ is primarily determined by interference, and a larger M is conducive to reducing the interference. Therefore, densely deployed mmWave UAV networks require large antenna arrays to overcome interference. According to Fig. 13, we further observe that there is an optimal N that maximizes $\mathbb{P}_{\mathrm{cov,b}}$, which is influenced by a combination of two factors. This observation aligns with the description of Fig. 6. Moreover, it is possible to perform a trade-off between N and M without affecting $\mathbb{P}_{\mathrm{cov,b}}$.

Fig. 14 demonstrates the trade-off that can be achieved between the height h and the number N of UAVs to achieve

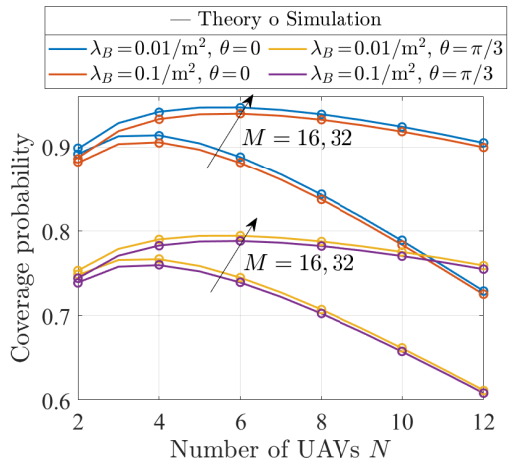

Fig. 13. Coverage probability $\mathbb{P}_{\mathrm{cov,b}}$ versus the number of UAVs N for different blockers and number of antenna elements M.

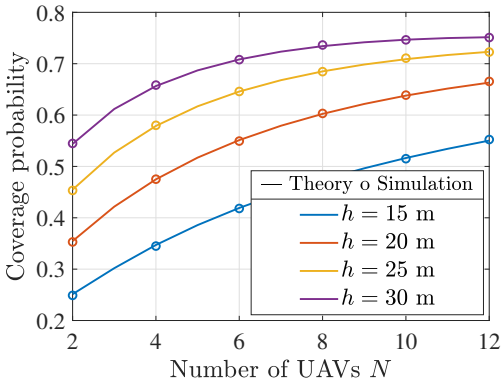

Fig. 14. Coverage probability $\mathbb{P}_{\mathrm{cov,b}}$ versus the number of UAVs N.

the typical coverage probability. Similar to the analysis of Fig. 7, the results in Fig. 14 indicate that increasing the height of UAVs can significantly reduce the required UAVs without affecting the coverage probability. Regarding deployment costs and network complexity, even if UAVs are deployed at higher altitudes, deploying fewer UAVs is more advantageous. However, higher UAVs altitudes may result in faster energy consumption. As a result, it is necessary to perform a trade-off between UAVs height and density when designing UAV.

Fig. 15 presents the variation of the coverage probability $\mathbb{P}_{\mathrm{cov,b}}$ with the communication range R for different numbers of UAVs N. As illustrated, there is an optimal R that maximizes $\mathbb{P}_{\mathrm{cov,b}}$. This is because when R is small, the UAV is in close proximity to the UE, resulting in significant interference in the channel. In such case, increasing R or reducing N can both mitigate interference and thereby increase the coverage probability. However, when R exceeds a certain range, the long transmission distance leads to serious path loss, thereby constraining $\mathbb{P}_{\mathrm{cov,b}}$. Therefore, there exists an optimal R that maximizes $\mathbb{P}_{\mathrm{cov,b}}$. Meanwhile, when R is large, increasing the number of UAVs can improve the probability of the serving UAV approaching the UE, thus shortening the communication distance and improving the coverage probability.

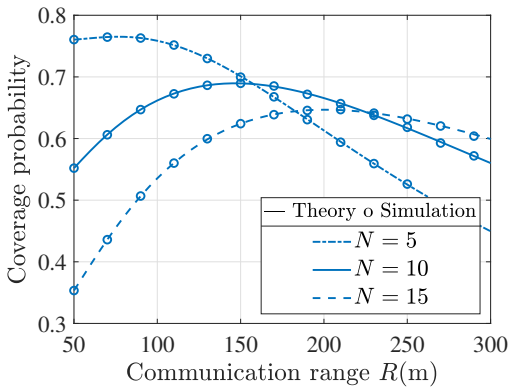

Fig. 15. Coverage probability $\mathbb{P}_{\mathrm{cov,b}}$ versus the communication range of UAVs R.

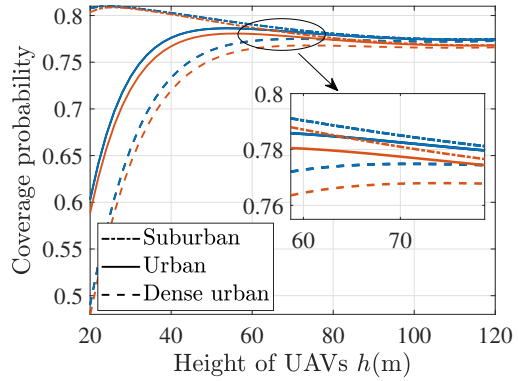

(a) Number of UAVs is small

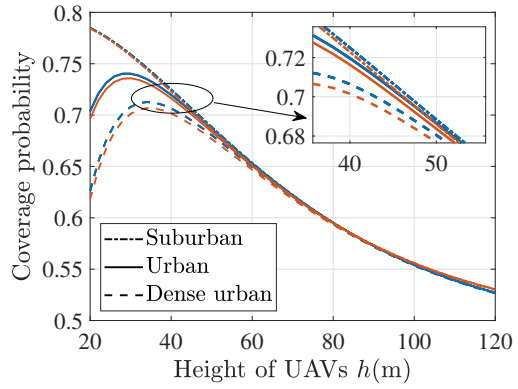

(b) Number of UAVs is large

Fig. 16. A comparison of $\mathbb{P}_{\mathrm{cov,b}}$ (blue curve) and $\mathbb{P}_{\mathrm{cov,p}}$ (red curve).

In Subsection V-A and V-B, the variation trends of $\mathbb{P}_{\mathrm{cov,p}}$ and $\mathbb{P}_{\mathrm{cov,b}}$ for different system design parameters are presented, respectively. The theoretical results agree well with the simulation results, which demonstrates the accuracy of our analysis model. After all, the coverage probability we derived can be used to evaluate and comparison the performance of mmWave UAV communication systems in various scenarios.

Fig. 16 presents a comparison between $\mathbb{P}_{\mathrm{cov,b}}$ and $\mathbb{P}_{\mathrm{cov,p}}$ from two UAVs models. To make a fair comparison, we assume that the density of UAVs under the two modes is

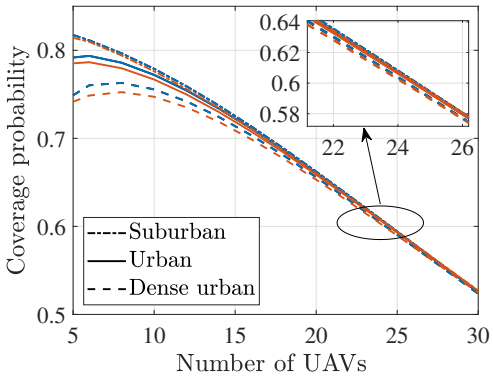

Fig. 17. A comparison of $\mathbb{P}_{\mathrm{cov,b}}$ (blue curve) and $\mathbb{P}_{\mathrm{cov,p}}$ (red curve) for different number of UAVs.

the same, i.e., $\lambda_T = \frac{N}{\pi R^2}$. Fig. 16(a) compares the coverage probabilities with $N = 8$, showing that $\mathbb{P}_{\mathrm{cov,b}}$ is higher for the BPP mode compared to $\mathbb{P}_{\mathrm{cov,p}}$ for the FHPPP mode. However, when $N = 18$, the difference between $\mathbb{P}_{\mathrm{cov,b}}$ and $\mathbb{P}_{\mathrm{cov,p}}$ becomes small and can be ignored, as shown in Fig. 16(b). The reason is that the main difference between these two models is that for FHPPP, the distribution of the number of UAVs N in disk $D(o,R)$ and its subregion is Poisson distributed, while for BPP, the number of UAVs N in $D(o,R)$ is fixed and in its subregion is binomial distributed [24], [41]. Furthermore, for large N, the binomial distribution can be approximated as a Poisson distribution [41]. Thus, for Fig. 16(b), $\mathbb{P}_{\mathrm{cov,p}}$ and $\mathbb{P}_{\mathrm{cov,b}}$ exhibit similar performance due to the consideration of a larger N. While for Fig. 16(a), the small N make it possible for there to be no UAVs at all in the actual Poisson process [24], resulting in $\mathbb{P}_{\mathrm{cov,p}}$ being equal to 0. Thus, the value of $\mathbb{P}_{\mathrm{cov,p}}$ is inferior to that of $\mathbb{P}_{\mathrm{cov,b}}$. Additionally, as h increases, the difference in coverage performance between the three scenarios becomes negligible due to the ability of the link to avoid static blockages. Fig. 17 further compares the trend of coverage probability under these two models, and the results are as expected. In summary, our results provide a theoretical basis for obtaining suitable UAV distribution models in different scenarios. Specifically, the BPP model is more suitable for covering a small-scale area with fewer UAVs, while the FHPPP model is advantageous for large-scale network deployment due to its tractability and not requiring knowledge of the specific number of UAVs required.

All the aforementioned finding indicate that human blockages do indeed affect the performance of air-to-ground mmWave UAV networks. Therefore, jointly considering multiple types of blockages helps to better design and evaluate such networks. Our study provides new insights into the evaluation of such networks. The results can be viewed as the coverage performance for mobile UAV scenarios at a specific moment. The UAV distribution model and LoS link model considered in this paper can also be applied to scenarios with more complex user distribution, access strategies, or multi-antenna systems. The relevant investigations will be included in our future work.

VI. Conclusions

This paper investigated the coverage performance of mmWave UAV networks by jointly considering dynamic, static, and self blockages, and incorporate two UAV distribution models. Consequently, our results enable the evaluation of the system performance under various scenarios. The tractable expression for the average LoS probability and coverage probability is obtained and verified by simulations. Our findings indicate that: (1) the coverage probability, average LoS probability, as well as average path loss are primarily influenced by static blockage and self-blockage at relatively low and high UAVs heights, respectively, while dynamic blockage cannot be ignored, especially when UAV is at relatively low heights and buildings are very sparse; (2) to avoid self-blockage, the UAV should be sufficiently high and the required height is proportional to the 2D distance of the UAV-UE link, and increases as the distance decreases; (3) BPP is more suitable for deploying a given number of UAVs to cover a small-scale area while FHPPP is more advantageous for large-scale deployments; (4) optimal deployment parameters exist to maximize the system performance.

Appendix A
Proof of Theorem 1

According to (20), the Laplace transform of aggregate interference I can first be expressed as

$$\mathcal{L}_I(s|r_{\mathrm{p}}) = \mathbb{E}\left[\exp\left(-s\sum_{j=1}^{N_{\mathrm{a}}} P_t G_u \zeta_k \ell_k(h,r_j)\right)\middle| r_{\mathrm{p}}\right]. \quad (30)$$

In the scenario we are considering, (30) can be rewritten as

$$\begin{aligned}\mathcal{L}_I(s|r_{\mathrm{p}}) &\overset{(a)}{=} \mathbb{E}_{N_{\mathrm{a}},R_j,\Psi}\left[\prod_{j=1}^{N_{\mathrm{a}}}\exp\left(-sP_tG_u\zeta_k\ell_k(h,r_j)\right)\middle| r_{\mathrm{p}}\right]\\ &\overset{(b)}{=} \mathbb{E}_{\hat{\Phi}}\left[\prod_{r_j\in\hat{\Phi}}\mathbb{E}_{\Psi}\left[\exp\left(-sP_tG_u\zeta_k\ell_k(h,r_j)\right)\right]\middle| r_{\mathrm{p}}\right]\\ &\overset{(c)}{=} \exp\left(-2\pi\lambda_T\int_{r_{\mathrm{p}}}^{R}\left(1-\mathbb{E}_{\Psi}\left[\exp\left(-sP_tG_u\zeta_k\ell_k(h,r_j)\right)\right]\right)\right.\\ &\qquad\left.\times r_j \mathrm{d}r_j\right), \end{aligned} \quad (31)$$

where step (a) performs the expectations of $\prod_{j=1}^{N_{\mathrm{a}}}\exp\left(-sP_tG_u\zeta_k\ell_k(h,r_j)\right)$ over the distributions of the number of interfering UAVs N_{a}, interfering distance R_j, path loss $\ell_k(h,r_j)$, Gamma variable $\zeta_k, k\in\{\mathrm{L},\mathrm{N}\}$, and antenna gain $G_u, u\in\{\mathrm{m},\mathrm{s}\}$. We define an indicator random variable Ψ to represent the channel statistical information, which includes the path loss $\ell_k(h,r_j)$, small-scale fading ζ_k, and antenna gain G_u. Step (b) depends on all UAVs are independent, and $\hat{\Phi} = \{r_1,\cdots,r_j,\cdots,r_{N_{\mathrm{a}}}\}$ is used to indicate the set of interference distances, which also follows the PPP model. Step (c) depends on the probability generating functional (PGFL) of PPP [32], i.e., $\mathbb{E}\left[\prod_{x\in\Phi}f(x)\right] = \exp\left(-\int_{\Phi}(1-f(x))\Lambda\mathrm{d}x\right)$

[48], [50], the integration from $r_{\rm p}$ to R since interfering UAVs are outside $D(o,r_{\rm p})$. Using (6), (7) and (8), we can get

$$\begin{aligned}&\mathbb{E}_{\Psi}\left[\exp\left(-sP_tG_u\zeta_k\ell_k(h,r_j)\right]\right.\\&\overset{\rm (a)}{=}\sum_{k\in\{\rm L,N\}}\mathbb{P}_k(h,r_j)\mathbb{E}_{\zeta_k,G_u}\left[\exp\left(-sP_tG_u\zeta_k\ell_k(h,r_j)\right)\right]\\&\overset{\rm (b)}{=}\sum_{k\in\{\rm L,N\}}\mathbb{P}_k(h,r_j)\sum_{u\in\{\rm m,s\}}\mathbb{P}_u\left(\frac{m_k}{m_k+sP_tG_u\ell_k(h,r_j)}\right)^{m_k},\end{aligned}\tag{32}$$

where $\mathbb{P}_k(h,r_j), k\in\{\rm L,N\}$ indicate the LoS/NLoS probability of the UAV-UE link. Therefore, step (a) follows the law of total probability, step (b) performs the expectation over the distributions of Gamma variable ζ_k, and antenna gain G_u according to [7], [32]. Finally, substituting (32) into (31), we can get the desired result, as shown in Theorem 1.

Appendix B
Proof of Corollary 1

In this case, the number of interfering UAVs is fixed, i.e., $N_{\rm a}=N-1$. Then, with the aid of (31), we have

$$\begin{aligned}\mathcal{L}_I(s|r_{\rm b})&=\mathbb{E}\left[\prod_{j=1}^{N-1}\mathbb{E}_{R_j,\Psi}\left[\exp\left(-sP_tG_u\zeta_k\ell_k(h,r_j)\right)\right]|r_{\rm b}\right]\\&=\left[\mathbb{E}_{R_j,\Psi}\left[\exp\left(-sP_tG_u\zeta_k\ell_k(h,r_j)\right)\right]|r_{\rm b}\right]^{N-1},\end{aligned}\tag{33}$$

where the last step follows from the fact that UAVs are i.i.d.. With the aid of (17), (32), and conditioned on $r_{\rm b}$, we have

$$\begin{aligned}&\mathbb{E}_{R_j,\Psi}\left[\exp\left(-sP_tG_u\zeta_k\ell_k(h,r_j)\right)\right]\\&=\int_{r_{\rm b}}^{R}\mathbb{E}_{\Psi}\left[\exp\left(-sP_tG_u\zeta_k\ell_k(h,r_j)\right)|r_j\right]f_{R_j}(r_j|r_{\rm b}){\rm d}r_j\\&=\int_{r_{\rm b}}^{R}\sum_{k\in\{\rm L,N\}}\mathbb{E}_{\zeta_k,G_u}\left[\exp\left(-sP_tG_u\zeta_k\ell_k(h,r_j)\right)|r_j\right]\\&\quad\times\mathbb{P}_k(h,r_j)\frac{2r_j}{R^2-r_{\rm b}^2}{\rm d}r_j\\&=\frac{2}{R^2-r_{\rm b}^2}\int_{r_{\rm b}}^{R}\sum_{k\in\{\rm L,N\}}\mathbb{P}_k(h,r_j)\sum_{u\in\{\rm m,s\}}\mathbb{P}_u\\&\quad\times\left(\frac{m_k}{m_k+sP_tG_u\ell_k(h,r_j)}\right)^{m_k}r_j{\rm d}r_j.\end{aligned}\tag{34}$$

Appendix C
Proof of Theorem 2

In this case, the PDF of the serving distance is denoted as $f_{R_{\rm p}}(r_{\rm p})$. Therefore, (23) can be rewritten as

$$\begin{aligned}\mathbb{P}_{\rm cov,p}&=\int_0^R\mathbb{P}\left({\rm SINR}>T|r_{\rm p}\right)f_{R_{\rm p}}(r_{\rm p}){\rm d}r_{\rm p}\\&=\int_0^R\sum_{k\in\{\rm L,N\}}\mathbb{P}_k(h,r_{\rm p})\mathbb{P}\left({\rm SINR}>T|r_{\rm p},k\right)f_{R_{\rm p}}(r_{\rm p}){\rm d}r_{\rm p},\end{aligned}\tag{35}$$

where $\mathbb{P}_{\rm L}(h,r_{\rm p})$ is the LoS probability of the link, which can be obtained according to (10), $\mathbb{P}_{\rm N}(h,r_{\rm p})=1-\mathbb{P}_{\rm L}(h,r_{\rm p})$. Therefore, step (a) follows the law of total probability. With the aid of (5), (6), (7), (8), (9), and (20), we first can obtain

$$\begin{aligned}&\int_0^R\mathbb{P}_{\rm L}(h,r_{\rm p})\mathbb{P}\left({\rm SINR}>T|r_{\rm p},{\rm L}\right)f_{R_{\rm p}}(r_{\rm p}){\rm d}r_{\rm p}\\&\overset{\rm (a)}{=}\int_0^R\mathbb{P}_{\rm L}(h,r_{\rm p})\mathbb{E}_I\left[\mathbb{P}\left(\zeta_{\rm L}>\frac{T(N_0+I)}{P_tG_{\rm m}\ell_{\rm L}(h,r_{\rm p})}\middle|r_{\rm p},I\right)\right]\\&\quad\times f_{R_{\rm p}}(r_{\rm p}){\rm d}r_{\rm p}\\&\overset{\rm (b)}{\geq}\int_0^R\left[1-\mathbb{E}_I\left[\left(1-\exp\left(\frac{-\xi_{\rm L}T(N_0+I)}{P_tG_{\rm m}\ell_{\rm L}(h,r_{\rm p})}\right)\right)^{m_{\rm L}}\middle|r_{\rm p}\right]\right]\\&\quad\times\mathbb{P}_{\rm L}(h,r_{\rm p})f_{R_{\rm p}}(r_{\rm p}){\rm d}r_{\rm p}\\&\overset{\rm (c)}{=}\int_0^R\left[1-\mathbb{E}_I\left[\sum_{m=0}^{m_{\rm L}}(-1)^mC_{m_{\rm L}}^m\exp\left(\frac{-m\xi_{\rm L}T(N_0+I)}{P_tG_{\rm m}\ell_{\rm L}(h,r_{\rm p})}\right)\middle|r_{\rm p}\right]\right]\\&\quad\times\mathbb{P}_{\rm L}(h,r_{\rm p})f_{R_{\rm p}}(r_{\rm p}){\rm d}r_{\rm p}\\&\overset{\rm (d)}{=}\int_0^R\mathbb{P}_{\rm L}(h,r_{\rm p})\sum_{m=1}^{m_{\rm L}}(\text{–}1)^{m+1}C_{m_{\rm L}}^m\exp\left(\frac{-m\xi_{\rm L}TN_0}{P_tG_{\rm m}\ell_{\rm L}(h,r_{\rm p})}\right)\\&\quad\times\mathcal{L}_I\left(\frac{m\xi_{\rm L}T}{P_tG_{\rm m}\ell_{\rm L}(h,r_{\rm p})}\middle|r_{\rm p}\right)f_{R_{\rm p}}(r_{\rm p}){\rm d}r_{\rm p},\end{aligned}\tag{36}$$

where step (a) follows the law of total probability, step (b) relies on a tight upper bound of the Gamma random variable $\zeta_{\rm L}$, i.e., $\mathbb{P}(\zeta_{\rm L}<\chi)\leq(1-e^{-\xi_{\rm L}\chi})^{m_{\rm L}}$ and $\xi_{\rm L}=m_{\rm L}(m_{\rm L}!)^{-1/m_{\rm L}}$ [51], $m_{\rm L}$ denotes a parameter of the Gamma distribution according to (6), step (c) depends on the Binomial theorem that $(1-x)^n=\sum_{i=0}^n(-1)^iC_n^ix^i$, and $\mathcal{L}_I\left(\frac{m\xi_{\rm L}T}{P_tG_{\rm m}\ell_{\rm L}(h,r_{\rm p})}\middle|r_{\rm p}\right)$ can be obtained by plugging $s=\frac{m\xi_{\rm L}T}{P_tG_{\rm m}\ell_{\rm L}(h,r_{\rm p})}$ into (21). Similarly

$$\begin{aligned}&\int_0^R\mathbb{P}_{\rm N}(h,r_{\rm p})\mathbb{P}\left({\rm SINR}>T|r_{\rm p},{\rm N}\right)f_{R_{\rm p}}(r_{\rm p}){\rm d}r_{\rm p}\\&\approx\int_0^R\mathbb{P}_{\rm N}(h,r_{\rm p})\sum_{m=1}^{m_{\rm N}}(\text{–}1)^{m+1}C_{m_{\rm N}}^m\exp\left(\frac{-m\xi_{\rm N}TN_0}{P_tG_{\rm m}\ell_{\rm N}(h,r_{\rm p})}\right)\\&\quad\times\mathcal{L}_I\left(\frac{m\xi_{\rm N}T}{P_tG_{\rm m}\ell_{\rm N}(h,r_{\rm p})}\middle|r_{\rm p}\right)f_{R_{\rm p}}(r_{\rm p}){\rm d}r_{\rm p},\end{aligned}\tag{37}$$

where $\xi_{\rm N}=m_{\rm N}(m_{\rm N}!)^{-1/m_{\rm N}}$. Substituting (12), (36), and (37) into (35), $\mathbb{P}_{\rm cov,p}$ can be obtained.

Appendix D
Proof of Corollary 2

In this case, (23) can first be rewritten as follows

$$\mathbb{P}_{\rm cov,b}=\int_0^R\sum_{k\in\{\rm L,N\}}\mathbb{P}_k(h,r_{\rm b})\mathbb{P}\left({\rm SINR}>T|r_{\rm b},k\right)f_{R_{\rm b}}(r_{\rm b}){\rm d}r_{\rm b},\tag{38}$$

following the same step as shown in (36), we can obtain

$$\begin{aligned}&\int_0^R\mathbb{P}_k(h,r_{\rm b})\mathbb{P}\left({\rm SINR}>T|r_{\rm b},k\right)f_{R_{\rm b}}(r_{\rm b}){\rm d}r_{\rm b}\\&\approx\int_0^R\mathbb{P}_k(h,r_{\rm b})\sum_{m=1}^{m_k}(\text{–}1)^{m+1}C_{m_k}^m\exp\left(\frac{-m\xi_kTN_0}{P_tG_{\rm m}\ell_k(h,r_{\rm b})}\right)\\&\quad\times\mathcal{L}_I\left(\frac{m\xi_kT}{P_tG_{\rm m}\ell_k(h,r_{\rm b})}\middle|r_{\rm b}\right)f_{R_{\rm b}}(r_{\rm b}){\rm d}r_{\rm b},k\in\{\rm L,N\}.\end{aligned}\tag{39}$$

Substituting (13) and (39) into (38), $\mathbb{P}_{\mathrm{cov,b}}$ can be obtained.

REFERENCES

[1] Y. Li and M. Xia, "Ground-to-Air Communications Beyond 5G: A Coordinated Multipoint Transmission Based on Poisson-Delaunay Triangulation," *IEEE Transactions on Wireless Communications*, vol. 22, no. 3, pp. 1841–1854, 2023.

[2] C. He, Y. Dong, and Z. J. Wang, "Radio Map Assisted Multi-UAV Target Searching," *IEEE Transactions on Wireless Communications*, vol. 22, no. 7, pp. 4698–4711, 2023.

[3] Y. Dong, C. He, and Z. J. Wang, "Dynamic Object Tracking by Multi-UAV with Time-variant Radio Maps," *IEEE Transactions on Wireless Communications*, pp. 1–1, 2023.

[4] H. Wang, H. Zhao, W. Wu, J. Xiong, D. Ma, and J. Wei, "Deployment Algorithms of Flying Base Stations: 5G and Beyond With UAVs," *IEEE Internet of Things Journal*, vol. 6, no. 6, pp. 10 009–10 027, 2019.

[5] Y. Su, X. Pang, W. Lu, N. Zhao, X. Wang, and A. Nallanathan, "Joint Location and Beamforming Optimization for STAR-RIS Aided NOMA-UAV Networks," *IEEE Transactions on Vehicular Technology*, vol. 72, no. 8, pp. 11 023–11 028, 2023.

[6] C. Ge, R. Zhang, D. Zhai, Y. Jiang, and B. Li, "UAV-Correlated MIMO Channels: 3-D Geometrical-Based Polarized Model and Capacity Analysis," *IEEE Internet of Things Journal*, vol. 10, no. 2, pp. 1446–1460, 2023.

[7] X. Shi and N. Deng, "Modeling and analysis of mmWave UAV swarm networks: A stochastic geometry approach," *IEEE Transactions on Wireless Communications*, vol. 21, no. 11, pp. 9447–9459, 2022.

[8] W. Yi, Y. Liu, and A. Deng, "Clustered UAV Networks With Millimeter Wave Communications: A Stochastic Geometry View," *IEEE Transactions on Communications*, vol. 68, no. 7, pp. 4342–4357, 2020.

[9] X. Pang, M. Liu, N. Zhao, Y. Chen, Y. Li, and F. R. Yu, "Secure Analysis in UAV-Based mmWave Relaying Networks with Cooperative Jamming," in *ICC 2021 - IEEE International Conference on Communications*, 2021, pp. 1–6.

[10] F. Li, C. He, X. Li, J. Peng, and K. Yang, "Geometric Analysis-Based 3D Anti-Block UAV Deployment for mmWave Communications," *IEEE Communications Letters*, vol. 26, no. 11, pp. 2799–2803, 2022.

[11] I. K. Jain, R. Kumar, and S. Panwar, "Driven by capacity or blockage? A millimeter wave blockage analysis," in *2018 30th International Teletraffic Congress (ITC 30)*, vol. 1. IEEE, 2018, pp. 153–159.

[12] I. K. Jain, R. Kumar, and S. S. Panwar, "The Impact of Mobile Blockers on Millimeter Wave Cellular Systems," *IEEE Journal on Selected Areas in Communications*, vol. 37, no. 4, pp. 854–868, 2019.

[13] Y. Kumar S and T. Ohtsuki, "Influence and Mitigation of Pedestrian Blockage at mmWave Cellular Networks," *IEEE Transactions on Vehicular Technology*, vol. 69, no. 12, pp. 15 442–15 457, 2020.

[14] M. F. Özkoç, A. Koutsaftis, R. Kumar, P. Liu, and S. S. Panwar, "The Impact of Multi-Connectivity and Handover Constraints on Millimeter Wave and Terahertz Cellular Networks," *IEEE Journal on Selected Areas in Communications*, vol. 39, no. 6, pp. 1833–1853, 2021.

[15] B. Han, L. Wang, and H. Schotten, "A 3D Human Body Blockage Model for Outdoor Millimeter-Wave Cellular Communication," *Physical Communication*, vol. 25, 10 2017.

[16] X. Pang, N. Zhao, J. Tang, C. Wu, D. Niyato, and K.-K. Wong, "IRS-assisted secure UAV transmission via joint trajectory and beamforming design," *IEEE Transactions on Communications*, vol. 70, no. 2, pp. 1140–1152, 2021.

[17] J. Zhao, J. Liu, J. Jiang, and F. Gao, "Efficient Deployment With Geometric Analysis for mmWave UAV Communications," *IEEE Wireless Communications Letters*, vol. 9, no. 7, pp. 1115–1119, 2020.

[18] C. Ma, X. Li, X. Xie, X. Ma, C. He, and Z. J. Wang, "Effects of Vertical Fluctuations on Air-to-Ground mmWave UAV Communications," *IEEE Wireless Communications Letters*, pp. 1–1, 2022.

[19] G. R. MacCartney, T. S. Rappaport, and S. Rangan, "Rapid Fading Due to Human Blockage in Pedestrian Crowds at 5G Millimeter-Wave Frequencies," in *GLOBECOM 2017 - 2017 IEEE Global Communications Conference*, 2017, pp. 1–7.

[20] H. Zhao, H. Wang, and J. Wu, "Deployment Algorithms for UAV Airborne Networks Toward On-Demand Coverage," *IEEE Journal on Selected Areas in Communications*, vol. 36, no. 9, pp. 2015–2031, 2018.

[21] M. Haenggi, J. G. Andrews, F. Baccelli, and M. Franceschetti, "Stochastic geometry and random graphs for the analysis and design of wireless networks," *IEEE Journal on Selected Areas in Communications*, vol. 27, no. 7, pp. 1029–1046, 2009.

[22] X. Wang, H. Zhang, Y. Tian, and V. C. M. Leung, "Modeling and Analysis of Aerial Base Station-Assisted Cellular Networks in Finite Areas Under LoS and NLoS Propagation," *IEEE Transactions on Wireless Communications*, vol. 17, no. 10, pp. 6985–7000, 2018.

[23] H. M. Jayaweera and S. Hanoun, "A Dynamic Artificial Potential Field (D-APF) UAV Path Planning Technique for Following Ground Moving Targets," *IEEE Access*, vol. 8, pp. 192 760–192 776, 2020.

[24] S. Srinivasa and M. Haenggi, "Distance Distributions in Finite Uniformly Random Networks: Theory and Applications," *IEEE Transactions on Vehicular Technology*, vol. 59, no. 2, pp. 940–949, 2010.

[25] C. Liu, M. Ding, C. Ma, Q. Li, Z. Lin, and Y.-C. Liang, "Performance Analysis for Practical Unmanned Aerial Vehicle Networks with LoS/NLoS Transmissions," in *2018 IEEE International Conference on Communications Workshops (ICC Workshops)*, 2018, pp. 1–6.

[26] W. Tang, H. Zhang, and Y. He, "Tractable Modelling and Performance Analysis of UAV Networks With 3D Blockage Effects," *IEEE Wireless Communications Letters*, vol. 9, no. 12, pp. 2064–2067, 2020.

[27] T. Hou, Y. Liu, Z. Song, X. Sun, and Y. Chen, "Exploiting NOMA for UAV Communications in Large-Scale Cellular Networks," *IEEE Transactions on Communications*, vol. 67, no. 10, pp. 6897–6911, 2019.

[28] C.-H. Liu, D.-C. Liang, M. A. Syed, and R.-H. Gau, "A 3D Tractable Model for UAV-Enabled Cellular Networks With Multiple Antennas," *IEEE Transactions on Wireless Communications*, vol. 20, no. 6, pp. 3538–3554, 2021.

[29] M. Alzenad and H. Yanikomeroglu, "Coverage and Rate Analysis for Vertical Heterogeneous Networks (VHetNets)," *IEEE Transactions on Wireless Communications*, vol. 18, no. 12, pp. 5643–5657, 2019.

[30] D. Kim, J. Lee, and T. Q. S. Quek, "Multi-layer Unmanned Aerial Vehicle Networks: Modeling and Performance Analysis," *IEEE Transactions on Wireless Communications*, vol. 19, no. 1, pp. 325–339, 2020.

[31] L. Yang, H. Zhang, and Y. He, "Temporal Correlation and Long-Term Average Performance Analysis of Multiple UAV-Aided Networks," *IEEE Internet of Things Journal*, vol. 8, no. 11, pp. 8854–8864, 2021.

[32] X. Guo, C. Zhang, F. Yu, and H. Chen, "Coverage Analysis for UAV-Assisted mmWave Cellular Networks Using Poisson Hole Process," *IEEE Transactions on Vehicular Technology*, vol. 71, no. 3, pp. 3171–3186, 2022.

[33] J. G. Andrews, R. K. Ganti, M. Haenggi, N. Jindal, and S. Weber, "A primer on spatial modeling and analysis in wireless networks," *Communications Magazine IEEE*, vol. 48, no. 11, pp. 156–163, 2010.

[34] S. M. Azimi-Abarghouyi, B. Makki, M. Haenggi, M. Nasiri-Kenari, and T. Svensson, "Stochastic Geometry Modeling and Analysis of Single- and Multi-Cluster Wireless Networks," *IEEE Transactions on Communications*, vol. 66, no. 10, pp. 4981–4996, 2018.

[35] M. Boschiero, M. Giordani, M. Polese, and M. Zorzi, "Coverage Analysis of UAVs in Millimeter Wave Networks: A Stochastic Geometry Approach," in *2020 International Wireless Communications and Mobile Computing (IWCMC)*, 2020, pp. 351–357.

[36] V. V. Chetlur and H. S. Dhillon, "Downlink Coverage Analysis for a Finite 3-D Wireless Network of Unmanned Aerial Vehicles," *IEEE Transactions on Communications*, vol. 65, no. 10, pp. 4543–4558, 2017.

[37] T. Z. H. Ernest, A. S. Madhukumar, R. P. Sirigina, and A. K. Krishna, "Impact of Cellular Interference on Uplink UAV Communications," in *2020 IEEE 91st Vehicular Technology Conference (VTC2020-Spring)*, 2020, pp. 1–5.

[38] S. Enayati, H. Saeedi, H. Pishro-Nik, and H. Yanikomeroglu, "Moving Aerial Base Station Networks: A Stochastic Geometry Analysis and Design Perspective," *IEEE Transactions on Wireless Communications*, vol. 18, no. 6, pp. 2977–2988, 2019.

[39] N. Cherif, M. Alzenad, H. Yanikomeroglu, and A. Yongacoglu, "Downlink Coverage and Rate Analysis of an Aerial User in Vertical Heterogeneous Networks (VHetNets)," *IEEE Transactions on Wireless Communications*, vol. 20, no. 3, pp. 1501–1516, 2021.

[40] N. Kouzayha, H. Elsawy, H. Dahrouj, K. Alshaikh, T. Y. Al-Naffouri, and M.-S. Alouini, "Analysis of Large Scale Aerial Terrestrial Networks with mmWave Backhauling," *IEEE Transactions on Wireless Communications*, vol. 20, no. 12, pp. 8362–8380, 2021.

[41] H. P. Keeler, "Binomial point process," https://hpaulkeeler.com/tag/binomial-point-process.

[42] C. Ma, X. Li, Y. Dong, and C. He, "Coverage Analysis For mmWAVE UAV Networks with Static and Dynamic Blockages," in *ICASSP 2024 - 2024 IEEE International Conference on Acoustics, Speech and Signal Processing (ICASSP)*, 2024, pp. 9211–9215.

[43] A. Al-Hourani, S. Kandeepan, and S. Lardner, "Optimal LAP Altitude for Maximum Coverage," *IEEE Wireless Communications Letters*, vol. 3, no. 6, pp. 569–572, 2014.

[44] M. T. Dabiri, M. Rezaee, V. Yazdanian, B. Maham, W. Saad, and C. S. Hong, "3D Channel Characterization and Performance Analysis of UAV-Assisted Millimeter Wave Links," *IEEE Transactions on Wireless Communications*, vol. 20, no. 1, pp. 110–125, 2021.
[45] K. Venugopal, M. C. Valenti, and R. W. Heath, "Device-to-Device Millimeter Wave Communications: Interference, Coverage, Rate, and Finite Topologies," *IEEE Transactions on Wireless Communications*, vol. 15, no. 9, pp. 6175–6188, 2016.
[46] M. Zouari, N. Baklouti, J. Sanchez-Medina, H. M. Kammoun, M. B. Ayed, and A. M. Alimi, "PSO-Based Adaptive Hierarchical Interval Type-2 Fuzzy Knowledge Representation System (PSO-AHIT2FKRS) for Travel Route Guidance," *IEEE Transactions on Intelligent Transportation Systems*, vol. 23, no. 2, pp. 804–818, 2022.
[47] B. Ahadzadeh, M. Abdar, F. Safara, A. Khosravi, M. B. Menhaj, and P. N. Suganthan, "SFE: A Simple, Fast, and Efficient Feature Selection Algorithm for High-Dimensional Data," *IEEE Transactions on Evolutionary Computation*, vol. 27, no. 6, pp. 1896–1911, 2023.
[48] J. G. Andrews, F. Baccelli, and R. K. Ganti, "A Tractable Approach to Coverage and Rate in Cellular Networks," *IEEE Transactions on Communications*, vol. 59, no. 11, pp. 3122–3134, 2011.
[49] H. ElSawy, A. Sultan-Salem, M.-S. Alouini, and M. Z. Win, "Modeling and Analysis of Cellular Networks Using Stochastic Geometry: A Tutorial," *IEEE Communications Surveys & Tutorials*, vol. 19, no. 1, pp. 167–203, 2017.
[50] D. Stoyan, W. S. Kendall, and J. Mecke, "Stochastic Geometry and Its Applications (Wiley Series in Probability and Statistics)," 1995.
[51] H. Alzer, "On some inequalities for the incomplete Gamma function ," *Mathematics of Computation of the American Mathematical Society*, vol. 55, no. 218, pp. 771–778, 1997.

Cunyan Ma received the B.Eng. degree in communication engineering from Northwest University, Xi'an, China, in 2019, where she is currently pursuing the Ph.D. degree in computer science. Her research interests includes UAV communications and millimeter wave transmission.

Xiaoya Li graduated from Xidian University with B.S. and Ph.D. degrees in communication and information system respectively in 2010 and 2016. Since Dec. 2016 she has been with the School of Information Science and Technology, Northwest University, Xi'an, China, where she is currently an Associate Professor. Her research interests focus on millimeter wave transmission, UAV communication, performance analysis, optimization and machine learning.

Chen He received the B.Eng. degree (*summa cum laude*) from McMaster University in 2007, and the M.A.Sc. and Ph.D. degrees from The University of British Columbia, Vancouver, in 2009 and 2014, respectively, all in electrical and computer engineering. He was a Research Engineer with Blackberry Limited, Canada, and a Post-Doctoral Research Fellow with UBC. He is currently a Full Professor with Northwest University, China. His research interests are the area of wireless communications, signal processing, and quantum information science. He is serving as an Associate Editor for the IEEE Signal Processing Letters.

Jinye Peng received the M.S. degree in computer science from Northwestern University, Xi'an, China, in 1996, and the Ph.D. degree from Northwestern Polytechnical University, Xi'an, in 2002. He joined Northwest University, in 2006, as a Professor. His research interests include image retrieval, face recognition, and machine learning.

Kun Yang received the Ph.D. from the Department of Electronic & Electrical Engineering of University College London (UCL), UK. He is currently a Chair Professor in the School of Computer Science Electronic Engineering, University of Essex, leading the Network Convergence Laboratory (NCL), UK. He is also an affiliated professor at UESTC, China. His main research interests include wireless networks and communications, IoT networking, data and energy integrated networks and mobile computing. He has published 300+ papers and filed 20 patents. He serves on the editorial boards of both IEEE and nonIEEE journals. He is an IEEE ComSoc Distinguished Lecturer (2020-2021).

Z. Jane Wang received the M.Sc. and Ph.D. degrees in electrical engineering from the University of Connecticut, in 2000 and 2002, respectively. She has been a Research Associate with the Electrical and Computer Engineering Department, University of Maryland, College Park. Since 2004, she has been with the Department Electrical and Computer Engineering, The University of British Columbia, Canada, where she is currently a Professor. Her research interests include statistical signal processing theory and applications. She received the Outstanding Engineering Doctoral Student Award. She co-received the EURASIP Journal on Applied Signal Processing Best Paper Award in 2004, and the IEEE Signal Processing Society Best Paper Award in 2005. She is the Chair and Founder of the IEEE Signal Processing Chapter at Vancouver. She is serving as an Associate Editor for the IEEE Transactions on Signal Processing, the IEEE Transactions on Information Forensics and Security, and the IEEE Transactions on Biomedical Engineering.